Single cell transcriptome profiling reveals pathogenesis of Bullous Pemphigoid

Guirong Liang[1], Chenjing Zhao[1], Qin Wei[1], Suying Feng[1*], Yetao Wang[1*]

1 Hospital for Skin Diseases, Institute of Dermatology, Chinese Academy of Medical Sciences and Peking Union Medical College, Nanjing, China

*Correspondence: fengsy@pumcderm.cams.cn; yetaowang@163.com

Abstract

Bullous pemphigoid (BP) triggers profound functional changes in both non-immune and immune cells in the skin and circulation, yet the underlying mechanisms remain elusive. In this study, we conducted single-cell transcriptome analysis on donor-matched lesional and non-lesional skin, as well as blood samples from BP patients. Lesional skin non-immune cells coordinately upregulated metabolism, wound healing, immune activation, and cell migration associated pathways. Skin LAMP3^{+} DCs derived from cDC2 exhibited higher pro-inflammatory signatures than those from cDC1, and VEGFA^{+} mast cells driving BP progression, were predominantly from lesional skin. As BP patients transition from active to remission stages, blood B cell function shifts from differentiation and memory formation to heightened type 1 interferon signaling and reduced IL-4 response. Blood CX3CR1^{+}ZNF683^{+} and LAG3^{+} exhausted T cells exhibited the highest TCR expansion among clones shared with skin CD8^{+}T cells, suggesting they likely represent BP-reactive cells fueling skin CD8^{+}T cell clonal expansion. Clinical parameters for BP severity correlated positively with blood NK cell IFN-γ production, whereas correlated negatively with NK cell AREG production. In lesional skin, NK cell-keratinocyte interactions exhibited reduced AREG-EGFR and enhanced IFNG-IFNGR1/2 signaling. NK cell-derived AREG mitigates IFN-γ-induced keratinocyte apoptosis, highlighting a crucial balance between AREG and IFN-γ in BP progression. These results reveal significant functional shifts in BP pathology within skin and blood cells and suggest new therapeutic targets for disease management.

Graphical abstract

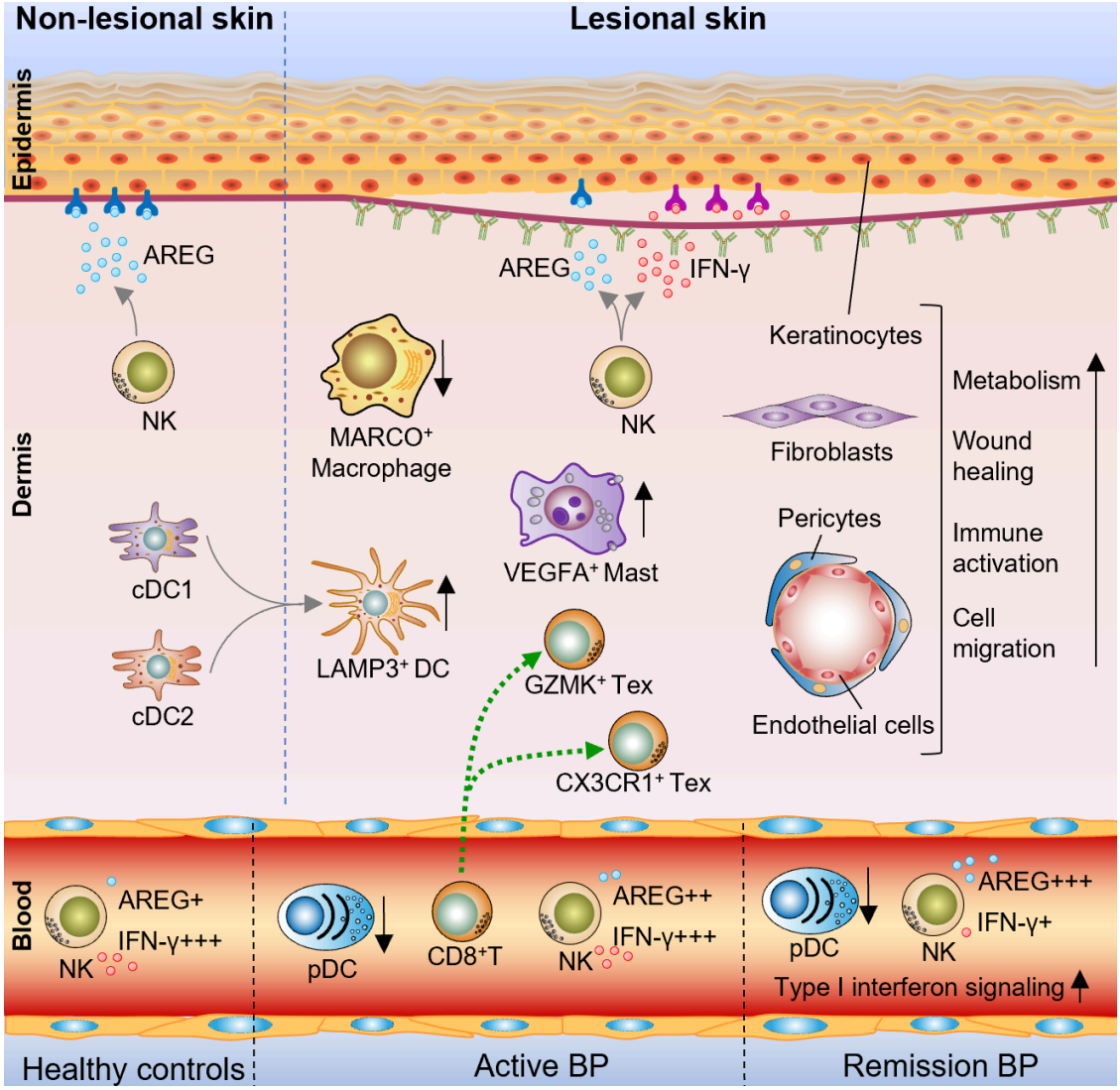

Introduction

Bullous pemphigoid (BP) is the most common autoimmune subepidermal blistering disease, induced by antibodies against hemidesmosome anchoring proteins BP180 and BP230 (encoded by COL17A1 and DST respectively) that links basal keratinocytes to the basement membrane zone[1,2]. BP is clinically characterized by intense pruritus and bullous lesions, and usually occurs in elderly (>60 years old)[3]. Increasing evidence shows that the influence of BP is systemic, the enhanced mortality is associated with multiple comorbidities, such as hematological abnormalities, tumors, cardiovascular diseases and neurological disorders[4–9]. However, the interrelationship between BP and its complications was not clear. Systematically investigating the pathological changes in the skin and other tissues may provide new insights that benefit the clinical control of disease progression.

Besides self-reactive antibodies, multiple cell types in the skin and the blood contributed to pathogenesis of BP. For example, the elevated activity of Th2 cells, type 2 innate lymphoid cells (ILC2s) and eosinophils contribute to blister formation and pruritus through production of IL-4, IL-5, IL-13, IL-31, MMP9, ROS and recruiting BP180 reactive IgE[1]. The absence of Treg cells lead to the generation of autoantibodies against BP230 in the BP mouse model[10]. Basophils, neutrophils and monocytes collectively determine BP progression in response to inflammatory cytokines or chemokines[11–13]. Natural killer (NK) cells enhance the inflammation of blistering skin disease by producing IFN-γ, TNF-α and releasing cytolytic granzymes[14–16]. Granzyme B cleaves BP180 and accumulates at dermal-epidermal junction, in blister fluid and in lesional skin of BP patients to promote disease progression[15,16], however, the regulatory role of blood NK cells is important to restrict type 2 inflammation in atopic dermatitis (AD)[17], indicating NK cells may play a paradoxical role in BP. Unbiased analysis of the cells in the skin and the peripheral blood mononuclear cells (PBMCs) should enhance the understanding of their contributions to BP pathology.

To reduce the comorbidities induced by exposure of pathogens and inflammatory irritants, the priority of BP treatment is to restore the homeostasis and integrity of lesional skin. The metabolism of keratinocytes and infiltrated immune cells is closely related with skin homeostasis[18,19], for example, aberrant activation of MTOR leads to enhanced proliferation of keratinocytes in psoriasis[20,21]. Inhibition of glycolysis using 2-deoxy-D-glucose (2-DG) ameliorates BP-like epidermolysis bullosa acquisita (EBA) in mouse model[22]. By regulating metabolic pathways, epidermal growth factor receptor (EGFR) signaling is pivotal for the survival, proliferation and differentiation of epithelial cells in normal and disease conditions[23]. We recently showed that human natural killer (NK) cells serve as a major innate source of amphiregulin (AREG)[24], a EGFR ligand playing important roles in maintaining the integrity of epithelium[25–27], whereas, the

function of AREG$^+$NK cells and their interplay with proinflammatory IFN-γ$^+$NK cells in BP remains unclear.

In this study, we conducted single-cell transcriptome analysis of paired lesional and non-lesional skin as well as donor-matched blood samples from BP patients. Our findings offer a detailed insight into the cellular dynamics in both skin and blood affected by BP, highlighting significant functional changes in immune and non-immune cells linked to the disease. These results indicate potential new targets for therapeutic intervention to enhance clinical treatment of BP.

Results

Experimental design and overview of single-Cell analysis of clinical BP samples

To understand the pathogenesis of BP, site and donor matched lesional (L) and non-lesional (NL) skin cells from untreated patients, PBMCs from skin samples matched BP patients in active or remission stage and from healthy donors were subjected to single cell transcriptome analysis (active BP was defined by the appearance of new skin lesions; remitted BP was defined by the healing of all lesions and the absence of new blisters or urticarial lesions for at least one month) (Figure 1A and Table S1). 113,044 cells from the skin and 38,854 cells from the blood were identified by Cell Ranger with an average depth of 45,095 mean reads/cell. After filtering by Seurat, 95,257 and 33,921 cells were identified from the skin and the blood respectively (Table S2 and Methods). Cells derived from the skin formed 12 clusters representing epidermal non-immune cells (keratinocytes, melanocytes), dermal non-immune cells (fibroblasts, endothelial cells, pericytes, vascular smooth muscle cells) and immune cells (T, B, NK, mast, dendritic cells and monophagocytes) in uniform manifold approximation and projection (UMAP) (Figures 1B and 1C). PBMCs derived from healthy donors and BP patients mainly formed 4 clusters representing T, B, NK cells and monophagocytes in UMAP (Figures 1B and 1C). Compared with non-lesional skin, the percentage of epidermal and dermal non-immune cells were not significantly altered (Figure 1D). Compared with healthy people, an increased monocytes and decreased lymphocytes percentage in the blood were detected in BP patients in both active and remission stages (Figures 1D and 1E), indicating an altered circulating immune environment in these patients.

Coordinated responses of non-immune cells in BP induced skin pathogenesis

Emerging evidence suggests that epidermal and dermal non-immune cells play pivotal roles in modulating immune responses in inflammatory skin diseases[28–31]. To explore

their transcriptional changes in BP, keratinocytes (KCs), fibroblasts (FBs), pericytes (PCs), and endothelial cells (ECs) from BP patients were reclustered (Figure S1A-S1D and 2A). Analysis of differentially expressed genes (DEgenes) between lesional and non-lesional skin revealed different clusters within each cell type showed varying responses to BP pathology (Figure 2B). For instance, differentiated KC2 had fewer unique DE genes compared to other KC clusters, while secretory-reticular and stressed FB had more unique DE genes than other FB clusters. In lesional skin, hair follicle-associated cells (HFACs) uniquely upregulated genes enriched in WNT signaling (CTNNB1, CTNNBIP1) and cell cycle regulation (CDK4), whereas stress response (EEF1A1, UBC) and metabolism of amino acids and lipid associated genes (LARS1, MPST, OSBP, PLPP2), were uniquely downregulated in differentiated KC1 (Table S3). Arterioles uniquely upregulated genes related to notch signaling (NOTCH4, JAG1, and JAG2), while venules upregulated genes associated with TGF-β signaling (TGFB1, LTBP3) and elastic fiber formation (ELN, FBLN2) (Table S3).

Our analysis revealed remarkable shared transcriptional changes among skin non-immune cell clusters. Notably, fibroblast and pericyte clusters had substantially more shared DE genes (681 and 629, respectively) compared to keratinocyte and endothelial cell clusters (115 and 82, respectively) (Figure 2B).

In keratinocyte clusters, the shared DEgenes play critical roles in inflammation and proliferation stage of wound healing[32], for instance, the upregulated genes in lesional skin were involved in regulating leukocyte aggregation (S100A8, S100A9, CD44), epithelial cell differentiation (SPRR1B, KRT16), growth (HBEGF, KRT17), migration (MYH9, RHOA) and adhesion (DSC2, CDH3), whereas, the downregulated genes were involved in regulation of apoptotic process (UBB, MYC), and cellular response to calcium (FOS, JUN) (Figure 2C and 2D). In fibroblast clusters, genes that function in tissue remodeling of injured skin, such as collagen synthesis (COL1A1, COL5A1), platelet aggregation (FLNA) were commonly upregulated in lesional skin. Additionally, collagen activated signaling pathway (COL1A1, COL4A1) was enriched by upregulated genes in pericytes clusters, indicating a crosstalk of these two cell types in BP lesional skin (Figure 2C and 2D). In endothelial cell clusters, genes associated with leukocyte migration (MYH9), chemotaxis (S100A8, S100A9) and wound healing (ENG, PPIA) were upregulated in lesional skin, highlighting their critical roles in regulating lymphocytes recruitment and inflammation (Figure 2C and 2D). Moreover, DEgenes associated with wound healing (PPIA, S100A8), response to stress (CEBPD, JUN), as well as glycolysis (GAPDH, PKM, PGAM1) and oxidative phosphorylation (NDUFA6, COX5A, UQCRQ) (excluding endothelial cells) were consistently detected across all skin non-immune cell types (Figure 2C and 2D).

The observed distinct and overlapping transcriptional responses among different skin non-immune cells in BP patients underscore their coordinated involvement in immune modulation, wound healing, and tissue remodeling in BP pathology. Gene Set Variation Analysis (GSVA) further elucidated these pathways, showing convergent transcriptional changes in KCs, FBs, PCs, and ECs affected by BP. In BP lesional skin, increased activity was commonly observed in pathways related to cellular metabolism, chemotaxis, immune activation, and cell migration (Figure 2E). Overall, these results offer a comprehensive insight into the transcriptional profiles of non-immune skin cells affected by BP.

The features of myeloid cells in BP patients

Myeloid cells play a significant role in creating the inflammatory environment associated with the formation of blisters and skin lesions in BP patients. In the skin, five subsets of macrophages (THBS1$^+$Mac, IER2$^+$Mac, STAB1$^+$Mac, MARCO$^+$Mac and TREM2$^+$Mac) and five subsets of dendritic cells (cDC1, cDC2, LAMP3$^+$DC, cycling DC and langerhans cells) have been identified (Figure 3A and 3C). Additionally, CD14$^+$ monocytes, CD16$^+$ monocytes, cDC, and pDC have been identified in the blood using established markers (Figure 3B and S2A)[33,34].

BP lesional skin showed a decrease in MARCO$^+$ macrophages compared to non-lesional skin (Figure 3D). Consistent with previous reports[35,36], these macrophages were involved in natural killer cell tolerance induction (HLA-E, LGALS9), negative regulation of neutrophil and macrophage activation (GRN, FCGR2B, VSIG4), dendritic cell differentiation (TMEM176A, FCGR2B), antigen presentation (FGL2, CD68, FCGR2B), and phagocytosis (AIF1, FCGR2B, MARCO, CD36), and were also involved in complement activation (C1QA, C1QC, CFD, SERPING1) and response to type 1 interferon (OAS1, IFI27, IFITM2, IFITM3) (Figure 3E).

Conversely, LAMP3$^+$DCs, which mature from conventional DCs[34], were increased in lesional skin (Figure 3D). Similar to the signatures identified in tumors, skin LAMP3$^+$DCs were enriched with genes associated with immunoregulation (CD274, PDCD1LG2, SOCS2), maturation (CD40, CD80, CD83), migration (MYO1G, CCR7, FSCN1), and Th2 response (IL4R, IL4I1, CCL17, CCL22) compared to cDC1 or cDC2 (Figures 3F and 3G). Furthermore, pseudotime analysis, akin to that of tumor LAMP3$^+$DCs[34], showed that skin LAMP3$^+$DCs were potentially derived from both cDC1s and cDC2s (Figure 3H).

The impact of BP pathology on LAMP3$^+$DCs derived from cDC1s and cDC2s was investigated next. In BP lesional skin, ISGs and S100A8/9 were commonly upregulated in both cDC1- and cDC2-derived LAMP3$^+$DCs, while chemokines attracting Th2 cells/eosinophils (CCL17, CCL18), the IgE receptor (FCER1G), and the costimulatory

molecule CD80 were uniquely upregulated in cDC2-derived LAMP3$^+$DCs (Figure 3I). Interestingly, chemokines recruiting neutrophils (CXCL2, CXCL3, CXCL8), TNF, MMPs (MMP9, MMP19), IgG/E receptors (FCGR2A, FCER1A), and complements (C3AR1, C5AR1) were highly expressed in cDC1- and/or cDC2-derived LAMP3$^+$DCs in non-lesional skin (Figure 3I). These findings indicate that cDC2-derived LAMP3$^+$DCs exhibit more proinflammatory features in BP lesional skin, while LAMP3$^+$DCs in non-lesional skin maintain a proinflammatory signature, suggesting an ongoing pathological process.

In BP patients, blood pDCs were decreased compared to healthy individuals, during both active and remission stages (Figure S2B and S2C). The DEgenes of blood pDCs in these stages exhibit a similar pattern compared to healthy individuals (Figure S2D). By analyzing the upregulated genes in top 10% of all DEgenes in pDCs from both stages revealed an 80% overlap in enriched pathways (Table S4), mainly involving TLR signaling (TLR8, CD14, ITGAM), IFN-γ signaling (FCGR1A, FCGR1B), antigen cross presentation (CD36, PSMB5), and neutrophil degranulation (C3AR1, S100A8, S100A9) (Figures S2E and S2F). Notably, CD14, CD36, S100A8, S100A9, FCGR1A showed even higher expression in pDCs from BP patients in remission stage compared to active stage, indicating a persistent proinflammatory signature in pDCs despite disease improvement (Figure S2D)

Four clusters of mast cells were identified in the skin of BP patients (Figures 4A and 4B). In general, genes associated with IL-2 signaling (IL2RA, IL2RG), type 2 inflammatory response (IL-4, IL-13, FCER1G), TNF signaling (TNFSF11, TNFRSF18), interferon signaling (IRF7, ISG15, IFITM3), leukocyte chemotaxis (CCL3, CCL4, CXCL8, CXCR4) and neutrophil degranulation (S100A8, S100A9), which are linked to the pathology of BP, were found to be upregulated in the lesional skin (Figures 4C and 4D). On the other hand, matrix metalloproteinases (MMP2, MMP14), which are crucial for blister formation[37], AP-1 family members (JUN, FOS) that regulate mast cell cytokine production[38], and IL1RL1 (ST2) signaling, which enhances the type 2 function of mast cells[39], were upregulated in non-lesion skin (Figures 4C and 4D). These findings indicate a switching of inflammatory features of mast cells during the transition from non-lesional to lesional skin.

TNF$^+$ and VEGFA$^+$ mast cells, linked to anti-tumor and pro-tumor activity respectively[33], displayed heightened proinflammatory features in lesional skin (Figure 4E). TNF$^+$ mast cells were mainly enriched with biological processes associated with translation (RPS15, RPS26, EEF1A1)) and cellular response to stress (HSPA1B, DNAJB1, FOS) (Figure S2G). Interestingly, VEGFA$^+$ mast cells, particularly enriched with pathways driving BP progression, such as neutrophil chemotaxis (CXCL8, C5AR1), IL-4, IL-13, and IFN-γ signaling (IL13, JAK1, STAT3, IFNGR1, IFNGR2, VEGFA, IRF1,

IRF7), and antigen presentation (HLA-A, HLA-B, HLA-E) (Figure 4F), were predominantly derived from lesional BP skin (Figure 4A), highlighting their critical roles in BP pathology.

The BP related transcriptional features of B cells

Consistent with prior research, skin B cells were rare (Figure 1B)[40], while blood B cells fell into four clusters: naive, TBX21$^+$, IgM$^+$ switched memory (SM), and SM (Figure S3A-S3B)[41,42]. We compared transcriptional features of B cells from healthy donors and BP patients in active and remission states (Figure S3C). B cells from BP patients commonly upregulated genes for NK and T cell interaction (CD48)[43], negative feedback of B cell activation (CD52)[44], and antigen presentation (HLA-A, HLA-B, HLA-DRB5). Active BP B cells upregulated genes for differentiation, memory, and preventing autoreactivity (CCR7, BACH2)[45,46], while down regulating IRF7, critical for type 1 interferon induction (Figure S3C). In contrast, B cells in remission stage uniquely upregulated type 1 interferon signaling genes (BST2, S100A8, S100A9, TLR10, IRF1, STAT1)[47], whereas genes involved in IL-4 response, IgM production, and cellular metabolism were downregulated (IL4R, IGHM, LAMTOR5) (Figure S3C). These findings delineate unique transcription profiles of B cells in BP patients, including shared upregulation of genes related to immune response, with active BP emphasizing B cell differentiation and memory, and remission showing heightened type 1 interferon signaling and reduced IL-4 response and IgM production.

Blood LAG3$^+$ and CX3CR1$^+$ZNF683$^+$ exhausted T cells represent BP reactive cells

It is well acknowledged that T cells play significant roles in BP progression through various mechanisms, including the production of itch mediators (IL-4, IL-13)[48], recruitment of eosinophils, regulating of autoantibody production by B cells[49], and modulation of inflammation and tissue damage[10]. During skin inflammation, blood T cells are a key source of the recruited T cells in the skin[50,51]. However, the detailed information regarding T cell subset clonal expansion, clone type sharing within the skin or between the skin and blood, which may have implications for potential therapeutic targets, remains unclear. To address these critical points, the transcriptome (including TCR) of paired skin and blood T cells from BP patients was examined (Figures 5A and S4A).

Our results revealed that Th1 cells were exclusively detected in the blood, whereas Th2 cells were found only in the skin (Figures 5A and S4A). Among CD4$^+$ T cells, Th2 cells exhibited the highest KI67 expression and proliferation score (Figures 5B and S4A), with higher scores in lesional skin than in non-lesional skin (Figure 5C), highlighting the pronounced activation of Th2 cells in the inflamed skin of BP patients. Except for Th1 cells, both skin and blood CD4$^+$T cell clusters showed limited clonal

expansion (Figures S4B-S4C), and inline with previous published reports[52], the sharing of clone types within or between skin and blood CD4$^+$T cell clusters was infrequent (Figures S5A-S5C).

In contrast to CD4$^+$T cells, expanded TCRs were readily detected in blood and skin CD8$^+$ T cell clusters, except for naive CD8$^+$T cells in the blood (Figures 5D and S5D). LAG3$^+$B3GAT1$^+$, LAG3$^+$B3GAT1$^-$ and CX3CR1$^+$ZNF683$^+$ exhausted T cells in the blood exhibited higher TCR expansion in both active or recovered BP patients compared with healthy people (Figure 5D), whereas the TCR expansion in lesional and non-lesional skin CD8$^+$T cells were largely comparable (Figure S5D). Shared clone types were more common in CD8$^+$T cells than in CD4$^+$T cells (Figures 5E, S5E and S5F). Moreover, we observed shared clone types between the paired skin and blood CD8$^+$T cells in active BP patients. For example, 7.64%, 13.19% and 6.25% of clone types of skin GZMK$^+$Tex cells were shared with blood CX3CR1$^+$ZNF683$^-$Tex, GZMK$^+$Tex and Tnv cells, respectively (Figure 5E). Additionally, 10.87% and 17.39% of clone types of skin CX3CR1$^+$Tex cells were shared with blood CX3CR1$^+$ZNF683$^+$ and CX3CR1$^+$ZNF683$^-$ exhausted T cell subsets, respectively (Figure 5E). Among these, blood CX3CR1$^+$ZNF683$^+$ and LAG3$^+$ exhaust T cells exhibited the highest clonal expansion in clone types shared with skin CD8$^+$T cells (Figure 5F), suggesting that these cells, with their increased fraction of expanded TCR clones in BP patients (Figure 5D), likely represent BP-reactive cells contributing to clonal expansion of skin CD8$^+$T cell .

Gene set analysis revealed increased TCR activity and cytotoxicity scores in CX3CR1$^+$ZNF683$^+$ and LAG3$^+$ Tex cells from all BP patients (Figure 5G). Remission-stage patients exhibited higher TCR activity compared to those in the active stage or in healthy donors, while cytotoxicity scores were consistent across all BP patients (Figure 5G). A heightened IFN response was observed in both CX3CR1$^+$ZNF683$^+$ and LAG3$^+$ Tex cells during remission, but only in CX3CR1$^+$ZNF683$^+$ Tex cells during the active stage (Figure 5G). These findings indicate that the features of BP-reactive CD8$^+$ T cells are further influenced by the stage of BP.

The activity of NK cells is associated with the disease progression of BP

Skin NK cells are primarily recruited from the circulation in response to inflammation and play a crucial role in the progression and resolution of skin diseases, including viral or bacterial infections and tumors[53,54]. NK cells from both lesional and non-lesional skin of BP patients, as well as from the blood of healthy individuals, BP patients in active and remission stages, were analyzed (Figure 6A). Unlike T cells, NK cells from the blood and skin were distinguished by their tissue origin (Figure 6B), confirming prior findings[53,54].

Skin NK cells were categorized into six distinct clusters. Notably, Cluster 0 (C0) NK cells had high levels of inflammatory cytokines and AP-1 family members (TNF, IFNG, ATF3, JUN), and C2 NK cells decreased in lesional skin exhibited high expression of cytotoxicity-associated genes (FCGR3A, GZMM and PRF1), whereas C4 NK cells exhibited high expression of AREG, an EGFR ligand known to promote immune tolerance and tissue repair[25], as well as inhibitory receptors KLRC1 (Figure 6C and S6A). Consistent with previous studies[24,55], blood NK cells were predominantly clustered into $CD56^{dim}$NK cells (C0 and C1) and $CD56^{hi}$NK cells (C2), which also exhibit high expression of AREG (Figure 6D).

Transcriptional features in BP pathology in NK cells from skin and blood were analyzed. In lesional skin, cytotoxicity-associated genes were downregulated in C1 and C2 NK cells (IFNGR1, FCER1G, NCR3, KLRB1) (Figure 6E, left). Conversely, various interferon-stimulated genes involved in infection prevention, were upregulated in different NK cell clusters (OASL, ISG20, IFITMs, DHX36), and AREG, crucial for maintaining homeostasis in inflamed tissue[25], was upregulated in C4 NK cells (Figure 6E, right), indicating a functional adaptation of NK cells in the lesional skin environment.

Compared with healthy individuals, the gene expression of blood NK cells affected by BP pathology were analyzed. Integrins (ITGB1, ITGB7), which promote epithelial residency, were upregulated in C1 and C2 NK cells during active and/or remission stages (Figure 6F). Cytotoxicity-associated genes (FCGR1G, IL12RB1, FCGR3A, GZMB, KLRF1, IFNG) were also upregulated in C1 and C2 NK cells during these stages, consistent with observations in BP-reactive $CD8^+$ T cells (Figures 5G and 6F). However, ISGs were upregulated in C0 (IFI35, IFITM3), C1 (IRF7), and C2 (ISG20, DDX58, IFI6) NK cells in the remission stage (Figure 6F). Interestingly, AREG expression was downregulated in BP active patients but recovered in the remission stage in C0 NK cells, suggesting the involvement of NK cells in skin lesion repair (Figure 6F). Given that blood NK cells serve as the primary source of NK cells in inflamed skin, the interplay between the observed pro-inflammatory and homeostasis features of blood NK cells may collectively contribute to BP pathogenesis.

The flow cytometry was performed to detect the percentage, and the inflammatory (IFN-γ) and homeostatic (AREG) cytokines production of blood NK cells (Figure 7A). The results revealed a decrease in both the percentage and number of NK cells in individuals with active BP (Figures 7B and S6B). However, in recovered individuals, the amount of NK cells was restored to levels comparable to healthy controls (Figure 7B and S6B). The AREG produced by total NK cells was increased in all BP patients, while IFN-γ production was decreased in recovered patients (Figures 7C, 7D, S6C and S6D). NK cells were further categorized into $AREG^+IFN\text{-}\gamma^-$, $AREG^+IFN\text{-}\gamma^+$ and $AREG^-IFN\text{-}\gamma^+$ subsets based on the distinct function of the two cytokines. Our findings revealed that

AREG$^+$NK cells, including AREG$^+$IFN-γ$^-$ and AREG$^+$IFN-γ$^+$ NK cells, were elevated in all BP patients (Figures 7E, 7F, S6E and S6F), whereas IFN-γ$^+$NK cells that did not produce AREG were reduced (Figure 7G and S6G).

The correlation between NK cell cytokine production profiles and BP clinical indicators, including bullous pemphigoid disease area index (BPDAI) and blister score[56], was examined. The percentage of total NK cells and AREG$^+$ NK cells showed a negative correlation with BPDAI, while IFN-γ$^+$NK cells exhibited a positive correlation with BP disease severity (Figures 7H-7J). Additionally, both subsets of AREG$^+$NK cell, including the percentage of AREG$^+$IFN-γ$^-$ and AREG$^+$IFN-γ$^+$ NK cells were negatively correlated with BPDAI, whereas the percentage of AREG$^-$IFN-γ$^+$ NK cells were positively correlated with BPDAI (Figures 7K-7M), suggesting that the IFN-γ and AREG produced by NK cells may play opposite roles in BP disease progression.

The pathology of BP primarily affects keratinocytes in the basal layer of the epidermis[1,2], where these cells are targeted by autoantibodies and further impacted by the inflammatory environment[1]. Cell chat analysis revealed that keratinocytes show the strongest ligand-receptor interactions with NK cells among all leukocytes (Figure S7A). The observation that IFNG-IFNGR1/2 signaling was enhanced, while AREG-EGFR signaling was decreased between NK cells and keratinocytes in BP lesional skin (Figure S7B), coupled with correlation analysis results (Figures 7H-7S), prompted us to investigate the biological impact of NK cell-produced AREG and IFN-γ on keratinocytes.

The survival of HaCaT epidermal keratinocytes cultured with supernatants from different NK cell cultures revealed significant differences (Figures 7T, 7U and S7C). Specifically, the IFN-γ from AREG$^-$IFN-γ$^+$NK cell culture supernatant induced notable cell death compared to DMEM alone or supernatant from AREG$^-$IFN-γ$^-$NK cell culture (Figure 7T). Conversely, HaCaT cells showed increased survival in AREG$^+$IFN-γ$^+$ than in AREG$^-$IFN-γ$^+$NK cell conditioned medium (Figure 7U), suggesting that AREG counteracts IFN-γ-induced apoptosis. The live or dead HaCaT cells percentage in AREG$^+$IFN-γ$^-$ conditioned medium was similar to DMEM alone (Figures 7T and 7U), indicating that the presence of AREG alone did not affect HaCaT cell survival. These experiments suggest AREG mitigates IFN-γ-induced apoptosis of keratinocytes during BP progression, potentially elucidating the negative correlation between AREG$^+$NK cells and the severity of the disease.

Discussion

Accelerating the wound healing of BP lesional skin is crucial for reducing the risk of pathogen infection and inflammatory irritants. This process requires complex

collaboration among skin structural cells. Beyond the unique features impacted by BP skin pathology, we observed that skin non-immune cells exhibited a coordinated response to BP-induced damage, with altered gene expression across different stages of wound healing (Figures 2C-2E). This may be regulated by their shared enriched pathways in the lesional skin, such as upregulated glycolysis, oxidative phosphorylation, and response to stress. Targeting these shared pathways may universally impact various types of skin structural cells to facilitate the healing of skin lesions. Supporting this notion, it has been reported that inhibiting glycolysis impairs wound healing, while high glucose treatment accelerates re-epithelialization in vitro [57]. Therefore, BP patients with metabolic disorders experiencing delayed healing of lesional skin may be further affected by additional metabolic inhibitor treatment.

The elevated activity of type 1 interferon signaling is closely associated with the susceptibility to autoimmune diseases such as systemic lupus erythematosus, Sjögren's syndrome, and rheumatoid arthritis [58]. Counterintuitively, we consistently observed an upregulation of type 1 interferon-associated genes in multiple blood cell populations of BP patients in the remission stage, including pDCs, B cells, $CD8^+$T cells, and NK cells (Figures S2D, S3C, 5G and 6F). However, type 1 interferon also has an anti-inflammatory mechanism due to its role in inducing immunosuppressive factors such as IL-10, SOCS1, and TTP, as well as inhibiting the expression of MMP genes[59,60], which would alleviate inflammation and facilitate disease improvement. Thus, the biological significance of this observation on BP disease progression warrants further research.

We have uncovered changes in the composition and function of several cell populations associated with BP pathology. For instance, immunosuppressive $MARCO^+$ macrophages were decreased, while $LAMP3^+$ DCs and $VEGFA^+$ mast cells, which are enriched with genes promoting Th2 responses and attracting eosinophils, were increased in the lesional skin (Figures 3F, 3G, and 4F). Identifying interventions that can reverse these alterations may be beneficial for alleviating BP-induced skin symptoms. Additionally, our analysis revealed that $LAG3^+$ and $CX3CR1^+ZNF683^+$ exhausted T cells in the blood share the highest expanded TCRs with skin $CD8^+$T cells. These cells also exhibited elevated TCR signaling and cytotoxicity scores in BP patients compared to healthy controls (Figures 5E, 5F, and 5G). Understanding their biological roles may provide new insights into the mechanisms of T cells in BP pathogenesis.

Traditionally, NK cells are recognized as proinflammatory cells that mediate tissue damage by producing IFN-γ and TNF-α[55]. However, our recent research revealed that, unlike mouse NK cells, human NK cells also serve as a major source of AREG, an EGFR ligand that plays critical roles in maintaining tissue homeostasis and immune tolerance[24]. Interestingly, clinical parameters measuring BP severity negatively

correlated with NK cell AREG production but positively correlated with their IFN-γ production, suggesting opposite functions of NK cell produced IFN-γ and AREG in BP disease progression (Figures 7H-7S). This observation is consistent with the increased $AREG^{+}IFN\text{-}\gamma^{-}$ NK cells and decreased $AREG^{-}IFN\text{-}\gamma^{+}$ NK cells in remission BP patients compared to active BP patients (Figures 7E-7G). In vitro experiments further confirmed that NK cell-produced AREG counteracts IFN-γ-induced apoptosis of epithelial cells (Figures 7T and 7U). Thus, inhibiting NK cell IFN-γ production and enhancing their AREG production could be a promising therapeutic strategy for BP.

Acknowledgments

This study was supported by CAMS Innovation Fund for Medical Sciences (CIFMS) (2024-I2M-3-005) and Hospital for Skin Diseases, Institute of Dermatology, Chinese Academy of Medical Sciences and Peking Union Medical College grant (3301030103119) to Yetao Wang. Scientific Research Project of Jiangsu Provincial Health Commission (ZD2021035) and Clinical and Translational Medicine Research Project of Chinese Academy of Medical Sciences (2023-I2M-C&T-B-112) to Suying Feng. We thank the study participants who provided skin and blood samples. All staff in the biobank of Institute of Dermatology, Chinese Academy of Medical Sciences, Jiangsu Biobank of Clinical Resources assisted with clinical sample collection. Guangzhou Genedenovo Biotechnology Co., Ltd assisted with sequencing data analysis.

Author contributions

Yetao Wang: Conceptualization; experiment design; data analysis; resources; supervision; validation; investigation; visualization; methodology; data curation; software; writing – original draft, review and editing; project administration; funding acquisition. Suying Feng: experiment design; resources; review and editing; Guirong Liang: experiment design, performing experiments; data analysis; validation; visualization, data curation; review and editing. Chenjing Zhao: data analysis; validation. Qin Wei: performing experiments.

Declaration of interests

All authors declare no competing interests.

Figure legends

Figure 1. Single cell atlas of BP skin and blood samples

(A) Experimental design of this study.

(B) UMAP of cells from four BP non-lesional and four lesional skin samples (left), and cells from PBMCs of two healthy donors, two active BP patients, and two remitted BP patients (right).

(C) The expression of cell type specific markers for (B).

(D) Histogram showing the percentage of $CD45^{-}$ and $CD45^{+}$ cells in BP non-lesional (n=4) and lesional skin (n=4), and the percentage of blood cells from healthy donors (n=2) and BP patients in active (n=2) and remission (n=2) stages.

(E) Percentage of monocytes (left) and lymphocytes (right) in PBMCs from healthy donors (n=10) and BP patients in active (n=12) and remission (n=12) stages by complete blood count. Two-tailed unpaired t test, ns, not significant, *, $p<0.05$; **, $p<0.01$. Data are mean with s.e.m.

Figure 2. Coordinated responses of non-immune cells in BP induced skin pathogenesis

(A) The expression of cell type specific markers for clusters of keratinocytes (KC), fibroblasts (FB), pericytes (PC) and endothelial cells (EC). Undifferentiated KC (undiff-KC), Proliferating KC (Prolif-KC), Differentiated KC1 (Diff-KC1), Differentiated KC2 (Diff-KC2), Hair follicle associated cells (HFAC), Secretory-papillary FB (SP-FB), Pro-inflammatory FB (Inf-FB), Stressed FB (Str-FB), Secretory-reticular FB (SR-FB), Mesenchymal FB (MES-FB), $THY1^{+}$ pericytes ($THY1^{+}$PC), THY1-$ACTA2^{high}$ pericytes ($ACTA2^{+}$PC), Intermediate pericytes (Inter-PC), Lymphatic endothelial cells (LEC), Post-arterial capillaries (PAC), Pre-venular capillaries (PVC), Post-capillary venules (PCV), Collecting venules (CV).

(B) Number of cluster unique and shared DEgenes between BP non-lesional and lesional KC, FB, PC and EC. The DEgenes was determined by Seurat FindAllMarkers ($P<0.05$, $Log_2FC>0.36$).

(C) Heatmap of cluster shared DEgenes between BP non-lesional and lesional KC, FB, PC and EC.

(D) Enriched pathways of cluster shared up-regulated (red) and down-regulated (blue) genes of KC, FB, PC, and EC in BP lesional skin by reactome analysis (FDR<0.05).

(F) GSVA of KC, FB, PC, and EC clusters in BP non-lesional and lesional skin.

Figure 3. Characterization of mononuclear phagocytes in BP patients

(A, B) UMAP of myeloid cells from BP non-lesional and lesional skin (A), and from the blood of healthy donors and BP patients in active and remission stages (B).

(C) Dot plot of specific markers for BP skin myeloid cell clusters.

(D) Percentage of myeloid cell clusters in BP non-lesional and lesional skin. Mann-Whitney test, ns, not significant; *, $p<0.05$. Data are mean with s.e.m.
(E, F) Enriched pathways of MARCO$^+$Mac (E) and LAMP3$^+$DC highly expressed genes by reactome analysis (FDR<0.05).
(G) The expression of genes associated with different functions among cDC1, cDC2 and LAMP3$^+$DC in the skin of BP patients
(H) Pseudotime analysis of BP skin DC subsets.
(I) Heatmap of inflammation-related DEgenes between BP non-lesional and lesional cDC1, cDC2, cDC1- and cDC2-derived LAMP3$^+$DC.

Figure 4. Characterization of mast cells in the skin of BP patients
(A) UMAP of non-lesional, lesional and total mast cells from the skin of BP patients.
(B) Dot plot showing specific markers for mast cell clusters.
(C) Enriched pathways of up-regulated (red) and down-regulated (blue) genes of mast cells in BP lesional skin by reactome analysis (FDR<0.05).
(D) Heatmap of DEgenes between BP non-lesional and lesional skin mast cells.
(E) Inflammatory response gene-set scores of mast cell clusters in BP non-lesional and lesional skin. Two-tailed paired t test, ns, not significant, **, $p<0.01$; ****, $p<0.0001$. Data are mean with s.e.m.
(F) Enriched pathways of VEGFA$^+$Mast cell highly expressed genes by reactome analysis (FDR<0.05).

Figure 5. Blood LAG3$^+$ and CX3CR1$^+$ZNF683$^+$ exhausted T cells represent BP reactive T cells
(A) UMAP of CD4$^+$ and CD8$^+$ T cells from BP non-lesional and lesional skin and from the blood of healthy donors and BP patients in active and remission stages.
(B) The proliferation scores of BP skin CD4$^+$T cell clusters.
(C) Proliferation scores of Th2 cells in BP lesional and non-lesional skin. Two-tailed paired t test, ***, $p<0.001$.
(D) Histogram showing the TCR expansion of blood CD8$^+$T cell clusters in healthy donors and BP patients in active and remission stages.
(E) Barplot showing the percentage of shared clone types between donor matched skin and blood CD8$^+$T cells in active BP patients.
(F) UMAP of mixed skin and blood CD8$^+$T cells (left) and clonal expansion in shared clone types between skin and blood CD8$^+$T cells (right) in active BP patients.
(G) Gene set analysis of blood CX3CR1$^+$ZNF683$^+$ and LAG3$^+$ Tex cells among healthy donors and BP patients in active and remission stages. Two-tailed unpaired t test, ns, not significant, *, $p<0.05$; **, $p<0.01$; ***, $p<0.001$. Data are mean with s.e.m.

Figure 6. Characterization of NK cells in BP patients

(A) UMAP of NK cells from BP non-lesional and lesional skin (left) and from the blood of healthy donors and BP patients in active and remission stages (right).
(B) UMAP of mixed skin (blue) and blood (red) NK cells.
(C, D) Dot plots showing specific markers for skin (C) and blood (D) NK cell clusters.
(E) Heatmap of cluster-specific DEgenes between BP non-lesional and lesional NK cells.
(F) Heatmap of cluster-specific DEgenes among blood NK cell clusters of healthy donors and BP patients in active and remission stages.

Figure 7. High AREG expression in BP blood NK cells correlates negatively with BP progression

(A) PBMCs were stimulated with IL-12 (10 ng/ml), IL-15 (50 ng/ml) and IL-18 (50 ng/ml) overnight, followed by incubation with protein transport inhibitor (1:1000 dilution) for 2 hrs in RPMI 1640 medium at 37°C with 5% CO_2. The production of AREG and IFN-γ by NK cells ($CD45^+Lin^-TBX21^+$) were detected by flow cytometry.
(B-G) Histograms showing the percentage of NK cells (B), and $AREG^+$ (C), IFN-γ^+ (D), $AREG^+$IFN-γ^- (E), $AREG^+$IFN-γ^+ (F) and $AREG^-$IFN-γ^+ (G) cells in total blood NK cells from healthy controls (n=37), BP patients in active (n=37) and remission (n=43) stages detected in (A).
(H-M) Pearson correlation of the percentage of blood NK cells (H, n=74), $AREG^+$ (I, n=75), IFN-γ^+ (G, n=71), $AREG^+$IFN-γ^- (K, n=72), $AREG^+$IFN-γ^+ (L, n=69) and $AREG^-$IFN-γ^+ (M, n=72) NK cells with BPDAI in BP patients.
(N-S) Pearson correlation of the percentage of blood NK cells (N, n=72), $AREG^+$ (O, n=73), IFN-γ^+ (P, n=72), $AREG^+$IFN-γ^- (Q, n=70), $AREG^+$IFN-γ^+ (R, n=68) and $AREG^-$IFN-γ^+ (S, n=72) NK cells with blister score in BP patients.
(T-U) NK cells were enriched with magnetic beads and were cultured in NK cell MACS medium for 10 days to generate $AREG^+$IFN-γ^- NK cells, or were further stimulated with IL-12 (10 ng/ml), IL-15 (50 ng/ml) and IL-18 (50 ng/ml) for 16 hrs to generate $AREG^+$IFN-γ^+ NK cells. The expanded NK cells were rested in MACS medium without supplement for 3 days to generate $AREG^-$IFN-γ^-NK cells, or were further stimulated with IL-12, IL-15 and IL-18 for 16 hrs to generate $AREG^-$IFN-γ^+ NK cells. All NK cells were then washed for 3 times, and were cultured in DMEM for 48 hrs to prepare the conditioned medium. HaCaT cells were cultured in conditioned medium for 48 hours, digested with TrypLE, and subjected to live/dead staining.
Each dot represents a unique donor, For (B-G, T and U), two-tailed unpaired t test, ns, not significant, *, $p<0.05$; **, $p<0.01$; ***, $p<0.001$. Data are mean with s.e.m.

Figure S1. UMAP of skin non-immune cells of BP patients

(A-D) UMAP of keratinocytes (A), fibroblasts (B), pericytes (C) and endothelial cells (D) from BP non-lesional and lesional skin.

Figure S2. Characterization of mononuclear phagocytes in BP patients

(A) Dot plot showing specific markers for blood myeloid cell clusters from healthy donors and BP patients in active and remission stages.

(B) Histogram showing the percentage of blood myeloid cell clusters from healthy donors (n=2) and BP patients in active (n=2) and remission (n=2) stages.

(C) Percentage of blood pDC cells from healthy donors (n=5) and BP patients in active (n=5) and remission (n=5) stages obtained from bulk RNA-seq data using CYBERSORTx. Mann-Whitney test, ns, not significant, *, $p<0.05$; **, $p<0.01$. Data are mean with s.e.m.

(D) Heatmap of DEgenes of blood pDCs among healthy donors and BP patients in active and remission stages.

(E, F) Enriched pathways of up-regulated genes in top 10% of all DEgenes by reactome analysis (FDR<0.05) in blood pDCs from BP patients in active (E) or remission (F) stages vs healthy donors.

(G) Enriched pathways of TNF^+Mast cell highly expressed genes by reactome analysis (FDR<0.05).

Figure S3. The BP related transcriptional features of B cells

(A) UMAP of B cells from the blood of healthy donors and BP patients in active and remission stages.

(B) Dot plot showing specific markers for blood B cell clusters.

(C) Heatmap of DEgenes of blood B cell clusters among healthy donors and BP patients in active and remission stages.

Figure S4. Characterization of T cells in BP patients

(A) Heatmaps showing specific markers for $CD4^+$ and $CD8^+$ T cell clusters from BP non-lesional and lesional skin and from the blood of healthy donors and BP patients in active and remission stages.

(B, C) Histogram showing the TCR expansion of $CD4^+$T cell clusters in BP non-lesional and lesional skin (B), and in the blood of healthy donors and BP patients in active and remission stages (C).

Figure S5. Characterization of T cells in BP patients

(A-C) Barplot showing the percentage of shared clone types in $CD4^+$T cell clusters from BP non-lesional and lesional skin (A), blood of healthy donors and BP patients in active and remission stages (B), and between donor matched skin and blood of active BP patients (C).

(D) Histogram showing the TCR expansion of $CD8^+$T cell clusters in BP non-lesional and lesional skin.
(E, F) Barplot showing the percentage of shared clone types in $CD8^+$T cell clusters from BP non-lesional and lesional skin (E), and blood of healthy controls and BP patients in active and remission stages (F).

Figure S6. High AREG expression in BP blood NK cells correlates negatively with BP progression
(A) Histograms showing the percentage of NK cell clusters from BP non-lesional and lesional skin (left, n=4), and from the blood of healthy donors (n=2) and BP patients in active (n=2) and remission stages (n=2) (right). Mann-Whitney test, *, $p<0.05$.
(B-G) Histograms showing the number of NK cells (B), and $AREG^+$ (C), IFN-γ^+ (D), $AREG^+$IFN-γ^- (E), $AREG^+$IFN-γ^+ (F) and $AREG^-$IFN-γ^+ (G) NK cells in one million live $CD45^+$ blood cells from healthy donors (n=37), BP patients in active (n=37) and remission (n=43) stages detected in (Figure 7A). Each dot represents a unique donor, two-tailed unpaired t test, ns, not significant, *, $p<0.05$; **, $p<0.01$; ***, $p<0.001$. Data are mean with s.e.m.

Figure S7. High AREG expression in BP blood NK cells correlates negatively with BP progression
(A) Network diagram of numbers of receptor-ligand pairs between keratinocytes and other immune cells in non-lesion and lesion of BP patients. The size of the peripheral circles indicates the number of receptor pairs contained within each subpopulation, the thickness of the lines represents the number of interacting receptor-ligand pairs between cells.
(B) Bubble plot showing the probability of ligand-receptor pairs between NK cells and keratinocytes. The size of the bubbles indicates the p-value, with smaller p-values resulting in larger bubbles. The color indicates the probability of communication.
(C) Flow cytometry detection of live and dead HaCaT cells in Figures 7T and 7U.

Methods

REAGENT or RESOURCE	SOURCE	IDENTIFIER
Antibodies		
Anti-Human CD3	Biolegend	Cat# 317306
Anti-Human CD4	Biolegend	Cat# 317408
Anti-Human TCRα/β	Biolegend	Cat# 306706
Anti-Human TCRγ/δ	Biolegend	Cat# 331208
Anti-Human CD19	Biolegend	Cat# 302206
Anti-Human CD20	Biolegend	Cat# 302304
Anti-Human CD22	Biolegend	Cat# 363508
Anti-Human CD14	Biolegend	Cat# 325604
Anti-Human CD34	ebioscience	Cat# 11-0349-42
Anti-Human FcεR1α	ebioscience	Cat# 11-5899-42
Anti-Human CD1a	Biolegend	Cat# 300104
Anti-Human CD11c	Biolegend	Cat# 301604
Anti-Human CD123	Biolegend	Cat# 306014
Anti-Human BDCA2	Biolegend	Cat# 354208
Anti-Human TBX21	ebioscience	Cat# 25-5825-82
Anti-Human IFN-γ	ebioscience	Cat# 17-7319-82
Anti-Human AREG	ebioscience	Cat# 12-5370-42
Anti-Human CD45	ebioscience	Cat# 56-9459-42
Biological Samples		
Skins	Biobank of Institute of Dermatology, Chinese Academy of Medical Sciences, Jiangsu Biobank of Clinical Resources (BM2015004)	
PBMCs	Biobank of Institute of Dermatology, Chinese Academy of Medical Sciences, Jiangsu Biobank of Clinical Resources (BM2015004)	
Blood for NK cells purification	Jiangsu province blood center	https://www.jsblood.com.cn/

Chemicals, Peptides, and Recombinant Proteins		
IL-2	Novoprotein	Cat# C013
IL-12	Novoprotein	Cat# CI58
IL-15	Novoprotein	Cat# C016
IL-18	Novoprotein	Cat# CH29
Protein transport inhibitor	ebioscience	Cat# 00-4980-03
TRIzol reagent	Invitrogen	Cat# 15596026CN
Fixable Viability Dye efluor 780	Invitrogen	Cat# 65-0865-18
Critical Commercial Assays		
EasySep Human NK Cell Isolation Kit	STEMCELL	Cat# 17955
NK MACS Medium human	MACS	Cat# 130-114-429
Chromium NextGEM Single Cell 5' HT Kit v2	10 X Genomics	Cat# PN-1000356
NEBNext Ultra RNA Library Prep Kit for Illumina	New England Biolabs	Cat# 7530
Deposited Data		
	NCBI Sequence Read Archive	
Software and Algorithms		
FlowJo	FlowJo, LLC	https://www.flowjo.com/
GraphPad Prism	GraphPad Software, Inc	https://www.graphpad.com/scientific-software/prism/
Cell Ranger	10x Genomics	https://support.10xgenomics.com/single-cell-gene-expression/software/pipelines/latest/what-is-cell-ranger
R Statistical Computing Software	The R Foundation	https://www.r-project.org/
GSVA	Hänzelmann, S. et al.[61]	https://www.bioconductor.org/packages/release/bioc/html/GSVA.html
Seurat 3.0	Stuart T. et al.[62]	http://satijalab.org/seurat/

Resource availability

For additional details and requests regarding resources and reagents, please contact the lead person, Yetao Wang (yetaowang@163.com).

Materials availability

This study did not produce novel or distinctive reagents.

Data availability

scRNA-Seq data of non-lesional and lesional skin of bullous pemphigoid (BP) and PBMCs from healthy controls and BP patients, and bulk RNA-Seq data of PBMCs from healthy controls and BP patients, are available in the NCBI Sequence Read Archive (SRA), BioProject: PRJNA1124631

Clinical samples

Samples of both non-lesional and lesional skin from BP patients, as well as PBMCs from both BP patients and healthy controls, were obtained from the biobank of the Institute of Dermatology, Chinese Academy of Medical Sciences, Jiangsu Biobank of Clinical Resources (BM2015004). Diagnostic criteria of BP: (1) intensely pruritic blisters of the skin, (2) positive linear IgG and/or C3c staining along the basement membrane zone by direct immunofluorescence, (3) positive IgG staining on the epidermal side of 1M-NaCl-split normal human skin by indirect immunofluorescence, (4) positive IgG enzyme-linked immunosorbent assay of BP180 NC16A and/or BP230 (MBL, Nagoya, Japan, >9 U/ml). BP was diagnosed if the first criterion and at least two of the last three criteria were met. Healthy blood samples used for NK cell purification were obtained from the Jiangsu Province Blood Center. All participants provided written informed consent following approval by the ethics committee of the Institute of Dermatology, Chinese Academy of Medical Sciences and Peking Union Medical College. Detailed clinical characteristics for each BP patient and healthy control are provided in Table S1.

Human skin cell preparation

To isolate single cells from both non-lesional and lesional skin of BP patients for scRNA-Seq, skin biopsies were processed using the instructions provided with the whole skin dissociation kit (130-101-540, MACS). Initially, fat tissue was removed by scraping, and the biopsies were then cut into small pieces (< 4 mm^2). Each piece underwent digestion in a buffer containing 435 µl buffer L, 12.5 µl enzyme P, 50 µl enzyme D, and 2.5 µl enzyme A on a 37°C shaker for 3 hrs. The digested skin tissue was subsequently diluted in ice-cold DMEM containing 2% BSA, filtered through a 70 µm strainer, and the flow-through was centrifuged at 300 x g for 10 min at 4°C. The isolated skin cells were finally resuspended in a MACS buffer (0.5% BSA + 2 mmol EDTA+1L PBS).

Peripheral blood mononuclear cells (PBMCs) isolation

Each human peripheral blood leukopak was initially washed with 80 ml of serum-free RPMI 1640 (Gibco), followed by layering onto lymphoprep (STEMCELL, 07851) and centrifugation at 500 x g for 30 min at room temperature. After three washes with MACS buffer, the isolated PBMCs were either used immediately or cryopreserved in FBS containing 10% DMSO.

Flow cytometry

PBMCs were initially stained with fixable viability dye efluor 780 (Invitrogen, 65-0865-18). For surface staining, cells were then incubated with antibodies in MACS buffer at 4°C for 30 minutes in the dark. For intracellular staining, cells were fixed and permeabilized using the Foxp3 staining kit (eBioscience, 00-5523-00), followed by staining for cytokines or TBX21 with antibodies in permeabilization buffer at 4°C for 30 minutes in the dark. The cells were ready for flow cytometry analysis after washing with MACS buffer.

scRNA-Seq library preparation

For scRNA-Seq library preparation, we utilized the Chromium NextGEM Single Cell 5' HT Kit v2 (10x Genomics, PN-1000356). Skin cells and PBMCs were washed and resuspended in 1x PBS containing 0.05% BSA. Cell count and viability were assessed using trypan blue staining under a microscope, with cell concentration adjusted to 1,000-2,000 cells/μl (viability > 80%). The single-cell suspension was loaded onto the Chromium Controller (10x Genomics) to encapsulate single cells into gel beads in emulsion (GEMs). The quality of amplified cDNA and the final sequencing library were assessed using the Agilent 2100 Expert (Agilent Technologies). Sequencing depth was maintained at approximately 30,000 mean reads per cell for skin cells and 70,000 mean reads per cell for PBMCs (Table S2). The libraries were sequenced using the Illumina NovaSeq 6000 platform.

scRNA-Seq data processing

113,044 skin cells and 38,854 PBMCs were identified by Cell Ranger (10x Genomics, version 5.0.0) with an average depth of 45,095 mean reads/cell (Table S2). A total of 95,527 cells (for skin) and 33,921 cells (for PBMCs) passed the filtering criteria using Seurat (Version 3.0) and were subsequently used for downstream analysis. The filtering criteria included: (1) ensuring nFeature ranged from 200 to 5900; (2) restricting UMIs to less than 49,000; and (3) ensuring UMIs from mitochondrial genes constituted less than 35% of the total UMIs. Cells derived from the skin were re-clustered into 12 unique clusters (res=0.5) and PBMCs derived from healthy donors and BP patients were mainly re-clustered into 4 clusters (res=0.5) for further analysis.

To identify genes highly expressed in a specific cluster, we compared their expression values with those of other clusters using the FindMarkers function in Seurat, employing the Model-based Analysis of Single-cell Transcriptomics (MAST) test. The average expression counts for each cluster were computed using the AverageExpression function.

Gene sets score analysis

The gene set scores for cell clusters were calculated using the AddModuleScore function in Seurat, with significance determined by either a Wilcoxon rank-sum test or a two-tailed unpaired t-test. Table S5 listed the signature genes for gene set score analysis.

Pseudotime analysis of BP skin DC subsets

To investigate the developmental pathways of LAMP3^{+} DCs, we utilized the Monocle algorithm (version 2.14.0) and focused on the top 400 signature genes identified by the differentialGeneTest function, The differentiation trajectory of DCs was inferred using Monocle with default parameters following dimension reduction and cell ordering.

Bulk RNA-Seq library preparation

Total RNA was isolated using the Trizol reagent kit (Invitrogen, Carlsbad, CA, USA) following the manufacturer's instructions. RNA integrity was evaluated with an Agilent 2100 Bioanalyzer and confirmed by RNase-free agarose gel electrophoresis. Subsequently, eukaryotic mRNA was enriched using Oligo(dT) beads. The enriched mRNA was then fragmented using a fragmentation buffer and reverse transcribed into cDNA using the NEBNext Ultra RNA Library Prep Kit for Illumina (NEB #7530, New England Biolabs, Ipswich, MA, USA). The resulting double-stranded cDNA fragments underwent end repair, addition of an A base, and ligation to Illumina sequencing adapters. After purification of the ligation reaction using AMPure XP Beads (1.0X), the cDNA fragments were PCR amplified. The prepared cDNA library was sequenced using Illumina Novaseq6000.

References

1. Genovese, G., Di Zenzo, G., Cozzani, E., Berti, E., Cugno, M., and Marzano, A.V. (2019). New Insights Into the Pathogenesis of Bullous Pemphigoid: 2019 Update. Front. Immunol. *10*, 1506.

2. Hammers, C.M., and Stanley, J.R. (2020). Recent Advances in Understanding Pemphigus and Bullous Pemphigoid. J. Invest. Dermatol. *140*, 733–741.

3. Bağcı, I.S., Horváth, O.N., Ruzicka, T., and Sárdy, M. (2017). Bullous pemphigoid. Autoimmun. Rev. *16*, 445–455.

4. Kibsgaard, L., Rasmussen, M., Lamberg, A., Deleuran, M., Olesen, A.B., and Vestergaard, C. (2017). Increased frequency of multiple sclerosis among patients with bullous pemphigoid: a population-based cohort study on comorbidities anchored around the diagnosis of bullous pemphigoid. Br. J. Dermatol. *176*, 1486–1491.

5. Pankakoski, A., Sintonen, H., Ranki, A., and Kluger, N. (2018). Comorbidities of bullous pemphigoid in a Finnish cohort. Eur. J. Dermatol. *28*, 157–161.

6. Yang, Y., Zhao, W., Yang, N., Cui, S., Jin, H., and Li, L. (2023). Associations between bullous pemphigoid and hematological diseases: Literature review on mechanistic connections and possible treatments. Front. Immunol. *14*, 1155181.

7. Taghipour, K., Chi, C.-C., Vincent, A., Groves, R.W., Venning, V., and Wojnarowska, F. (2010). The association of bullous pemphigoid with cerebrovascular disease and dementia: a case-control study. Arch. Dermatol. *146*, 1251–1254.

8. Papakonstantinou, E., Limberg, M.M., Gehring, M., Kotnik, N., Kapp, A., Gibbs, B.F., and Raap, U. (2019). Neurological disorders are associated with bullous pemphigoid. J. Eur. Acad. Dermatol. Venereol. *33*, 925–929.

9. Hu, F.-X., Liang, J.-Q., Nur, D.-L., Wu, C.-Y., and Kang, X.-J. (2020). A case of bullous pemphigoid with nail damage associated with Kaposi sarcoma. Int. J. Dermatol. Venereol. *Publish Ahead of Print*, 1.

10. Haeberle, S., Wei, X., Bieber, K., Goletz, S., Ludwig, R.J., Schmidt, E., Enk, A.H., and Hadaschik, E.N. (2018). Regulatory T-cell deficiency leads to pathogenic bullous pemphigoid antigen 230 autoantibody and autoimmune bullous disease. J. Allergy Clin. Immunol. *142*, 1831–1842.e7.

11. de Graauw, E., Sitaru, C., Horn, M.P., Borradori, L., Yousefi, S., Simon, D., and Simon, H.-U. (2018). Monocytes enhance neutrophil-induced blister formation in an ex vivo model of bullous pemphigoid. Allergy *73*, 1119–1130.

12. Kimura, R., Sugita, K., Horie, T., and Yamamoto, O. (2022). Dual role of basophils in the pathogenesis of bullous pemphigoid elucidated by pathological and

ultrastructural studies. Eur. J. Dermatol. *32*, 322–333.

13. Limberg, M.M., Weihrauch, T., Gray, N., Ernst, N., Hartmann, K., and Raap, U. (2023). Eosinophils, Basophils, and Neutrophils in Bullous Pemphigoid. Biomolecules *13*. 10.3390/biom13071019.

14. Zakka, L.R., Fradkov, E., Keskin, D.B., Tabansky, I., Stern, J.N.H., and Ahmed, A.R. (2012). The role of natural killer cells in autoimmune blistering diseases. Autoimmunity *45*, 44–54.

15. Hiroyasu, S., Zeglinski, M.R., Zhao, H., Pawluk, M.A., Turner, C.T., Kasprick, A., Tateishi, C., Nishie, W., Burleigh, A., Lennox, P.A., et al. (2021). Granzyme B inhibition reduces disease severity in autoimmune blistering diseases. Nat. Commun. *12*, 302.

16. Russo, V., Klein, T., Lim, D.J., Solis, N., Machado, Y., Hiroyasu, S., Nabai, L., Shen, Y., Zeglinski, M.R., Zhao, H., et al. (2018). Granzyme B is elevated in autoimmune blistering diseases and cleaves key anchoring proteins of the dermal-epidermal junction. Sci. Rep. *8*, 9690.

17. Mack, M.R., Brestoff, J.R., Berrien-Elliott, M.M., Trier, A.M., Yang, T.-L.B., McCullen, M., Collins, P.L., Niu, H., Bodet, N.D., Wagner, J.A., et al. (2020). Blood natural killer cell deficiency reveals an immunotherapy strategy for atopic dermatitis. Sci. Transl. Med. *12*. 10.1126/scitranslmed.aay1005.

18. Haensel, D., Jin, S., Sun, P., Cinco, R., Dragan, M., Nguyen, Q., Cang, Z., Gong, Y., Vu, R., MacLean, A.L., et al. (2020). Defining Epidermal Basal Cell States during Skin Homeostasis and Wound Healing Using Single-Cell Transcriptomics. Cell Rep. *30*, 3932–3947.e6.

19. Cibrian, D., de la Fuente, H., and Sánchez-Madrid, F. (2020). Metabolic Pathways That Control Skin Homeostasis and Inflammation. Trends Mol. Med. *26*, 975–986.

20. Buerger, C., Malisiewicz, B., Eiser, A., Hardt, K., and Boehncke, W.H. (2013). Mammalian target of rapamycin and its downstream signalling components are activated in psoriatic skin. Br. J. Dermatol. *169*, 156–159.

21. Wang, J., Cui, B., Chen, Z., and Ding, X. (2022). The regulation of skin homeostasis, repair and the pathogenesis of skin diseases by spatiotemporal activation of epidermal mTOR signaling. Front Cell Dev Biol *10*, 950973.

22. Schilf, P., Schmitz, M., Derenda-Hell, A., Thieme, M., Bremer, T., Vaeth, M., Zillikens, D., and Sadik, C.D. (2021). Inhibition of Glucose Metabolism Abrogates the Effector Phase of Bullous Pemphigoid-Like Epidermolysis Bullosa Acquisita. J. Invest. Dermatol. *141*, 1646–1655.e3.

23. Chen, J., Zeng, F., Forrester, S.J., Eguchi, S., Zhang, M.-Z., and Harris, R.C. (2016). Expression and Function of the Epidermal Growth Factor Receptor in

Physiology and Disease. Physiol. Rev. *96*, 1025–1069.

24. Wang, Y., Lifshitz, L., Silverstein, N.J., Mintzer, E., Luk, K., StLouis, P., Brehm, M.A., Wolfe, S.A., Deeks, S.G., and Luban, J. (2023). Transcriptional and chromatin profiling of human blood innate lymphoid cell subsets sheds light on HIV-1 pathogenesis. EMBO J. *42*, e114153.

25. Zaiss, D.M.W., Gause, W.C., Osborne, L.C., and Artis, D. (2015). Emerging functions of amphiregulin in orchestrating immunity, inflammation, and tissue repair. Immunity *42*, 216–226.

26. Cox, J.R., Cruickshank, S.M., and Saunders, A.E. (2021). Maintenance of Barrier Tissue Integrity by Unconventional Lymphocytes. Front. Immunol. *12*, 670471.

27. Krishnan, S., Prise, I.E., Wemyss, K., Schenck, L.P., Bridgeman, H.M., McClure, F.A., Zangerle-Murray, T., O'Boyle, C., Barbera, T.A., Mahmood, F., et al. (2018). Amphiregulin-producing γδ T cells are vital for safeguarding oral barrier immune homeostasis. Proc. Natl. Acad. Sci. U. S. A. *115*, 10738–10743.

28. Sisto, M., and Lisi, S. (2023). Immune and Non-Immune Inflammatory Cells Involved in Autoimmune Fibrosis: New Discoveries. J. Clin. Med. Res. *12*. 10.3390/jcm12113801.

29. Kamata, M., and Tada, Y. (2023). Crosstalk: keratinocytes and immune cells in psoriasis. Front. Immunol. *14*, 1286344.

30. Xu, Z., Chen, D., Hu, Y., Jiang, K., Huang, H., Du, Y., Wu, W., Wang, J., Sui, J., Wang, W., et al. (2022). Anatomically distinct fibroblast subsets determine skin autoimmune patterns. Nature *601*, 118–124.

31. Layton, T.B., Williams, L., Yang, N., Zhang, M., Lee, C., Feldmann, M., Trujillo, G., Furniss, D., and Nanchahal, J. (2022). A vasculature niche orchestrates stromal cell phenotype through PDGF signaling: Importance in human fibrotic disease. Proc. Natl. Acad. Sci. U. S. A. *119*, e2120336119.

32. Piipponen, M., Li, D., and Landén, N.X. (2020). The Immune Functions of Keratinocytes in Skin Wound Healing. Int. J. Mol. Sci. *21*. 10.3390/ijms21228790.

33. Cheng, S., Li, Z., Gao, R., Xing, B., Gao, Y., Yang, Y., Qin, S., Zhang, L., Ouyang, H., Du, P., et al. (2021). A pan-cancer single-cell transcriptional atlas of tumor infiltrating myeloid cells. Cell *184*, 792–809.e23.

34. Zhang, Q., He, Y., Luo, N., Patel, S.J., Han, Y., Gao, R., Modak, M., Carotta, S., Haslinger, C., Kind, D., et al. (2019). Landscape and Dynamics of Single Immune Cells in Hepatocellular Carcinoma. Cell *179*, 829–845.e20.

35. La Fleur, L., Botling, J., He, F., Pelicano, C., Zhou, C., He, C., Palano, G., Mezheyeuski, A., Micke, P., Ravetch, J.V., et al. (2021). Targeting MARCO and

IL37R on Immunosuppressive Macrophages in Lung Cancer Blocks Regulatory T Cells and Supports Cytotoxic Lymphocyte Function. Cancer Res. *81*, 956–967.

36. Jing, J., Yang, I.V., Hui, L., Patel, J.A., Evans, C.M., Prikeris, R., Kobzik, L., O'Connor, B.P., and Schwartz, D.A. (2013). Role of macrophage receptor with collagenous structure in innate immune tolerance. J. Immunol. *190*, 6360–6367.

37. Cirillo, N., and Prime, S.S. (2021). A Scoping Review of the Role of Metalloproteinases in the Pathogenesis of Autoimmune Pemphigus and Pemphigoid. Biomolecules *11*. 10.3390/biom11101506.

38. Srivastava, M., and Kaplan, M.H. (2021). Transcription Factors in the Development and Pro-Allergic Function of Mast Cells. Front Allergy *2*, 679121.

39. Griesenauer, B., and Paczesny, S. (2017). The ST2/IL-33 Axis in Immune Cells during Inflammatory Diseases. Front. Immunol. *8*, 475.

40. Egbuniwe, I.U., Harris, R.J., Nakamura, M., Nestle, F.O., Akbar, A.N., Karagiannis, S.N., and Lacy, K.E. (2022). B Lymphocytes Accumulate and Proliferate in Human Skin at Sites of Cutaneous Antigen Challenge. J. Invest. Dermatol. *142*, 726–731.e4.

41. Ota, M., Nakano, M., Nagafuchi, Y., Kobayashi, S., Hatano, H., Yoshida, R., Akutsu, Y., Itamiya, T., Ban, N., Tsuchida, Y., et al. (2023). Multimodal repertoire analysis unveils B cell biology in immune-mediated diseases. Ann. Rheum. Dis. *82*, 1455–1463.

42. Sanz, I., Wei, C., Jenks, S.A., Cashman, K.S., Tipton, C., Woodruff, M.C., Hom, J., and Lee, F.E.-H. (2019). Challenges and Opportunities for Consistent Classification of Human B Cell and Plasma Cell Populations. Front. Immunol. *10*, 2458.

43. McArdel, S.L., Terhorst, C., and Sharpe, A.H. (2016). Roles of CD48 in regulating immunity and tolerance. Clin. Immunol. *164*, 10–20.

44. Bhamidipati, K., Silberstein, J.L., Chaichian, Y., Baker, M.C., Lanz, T.V., Zia, A., Rasheed, Y.S., Cochran, J.R., and Robinson, W.H. (2020). CD52 Is Elevated on B cells of SLE Patients and Regulates B Cell Function. Front. Immunol. *11*, 626820.

45. Jang, E., Kim, U.K., Jang, K., Song, Y.S., Cha, J.-Y., Yi, H., and Youn, J. (2019). Bach2 deficiency leads autoreactive B cells to produce IgG autoantibodies and induce lupus through a T cell-dependent extrafollicular pathway. Exp. Mol. Med. *51*, 1–13.

46. Mcheik, S., Van Eeckhout, N., De Poorter, C., Galés, C., Parmentier, M., and Springael, J.-Y. (2019). Coexpression of CCR7 and CXCR4 During B Cell Development Controls CXCR4 Responsiveness and Bone Marrow Homing. Front. Immunol. *10*, 2970.

47. Wiedemann, G.M., Santosa, E.K., Grassmann, S., Sheppard, S., Le Luduec, J.-B., Adams, N.M., Dang, C., Hsu, K.C., Sun, J.C., and Lau, C.M. (2021). Deconvoluting global cytokine signaling networks in natural killer cells. Nat. Immunol. *22*, 627–638.

48. Hashimoto, T., Kursewicz, C.D., Fayne, R.A., Nanda, S., Shah, S.M., Nattkemper, L., Yokozeki, H., and Yosipovitch, G. (2020). Pathophysiologic mechanisms of itch in bullous pemphigoid. J. Am. Acad. Dermatol. *83*, 53–62.

49. Li, Q., Liu, Z., Dang, E., Jin, L., He, Z., Yang, L., Shi, X., and Wang, G. (2013). Follicular helper T Cells (Tfh) and IL-21 involvement in the pathogenesis of bullous pemphigoid. PLoS One *8*, e68145.

50. Hirai, T., Whitley, S.K., and Kaplan, D.H. (2020). Migration and Function of Memory CD8+ T Cells in Skin. J. Invest. Dermatol. *140*, 748–755.

51. Sabat, R., Wolk, K., Loyal, L., Döcke, W.-D., and Ghoreschi, K. (2019). T cell pathology in skin inflammation. Semin. Immunopathol. *41*, 359–377.

52. Ruan, Y., Xu, C., Zhang, T., Zhu, L., Wang, H., Wang, J., Zhu, H., Huang, C., and Pan, M. (2024). Single-Cell Profiling Unveils the Inflammatory Heterogeneity within Cutaneous Lesions of Bullous Pemphigoid. J. Invest. Dermatol. 10.1016/j.jid.2024.02.029.

53. Torcellan, T., Friedrich, C., Doucet-Ladevèze, R., Ossner, T., Solé, V.V., Riedmann, S., Ugur, M., Imdahl, F., Rosshart, S.P., Arnold, S.J., et al. (2024). Circulating NK cells establish tissue residency upon acute infection of skin and mediate accelerated effector responses to secondary infection. Immunity *57*, 124–140.e7.

54. Tang, F., Li, J., Qi, L., Liu, D., Bo, Y., Qin, S., Miao, Y., Yu, K., Hou, W., Li, J., et al. (2023). A pan-cancer single-cell panorama of human natural killer cells. Cell *0*. 10.1016/j.cell.2023.07.034.

55. Wang, Y., Lifshitz, L., Gellatly, K., Vinton, C.L., Busman-Sahay, K., McCauley, S., Vangala, P., Kim, K., Derr, A., Jaiswal, S., et al. (2020). HIV-1-induced cytokines deplete homeostatic innate lymphoid cells and expand TCF7-dependent memory NK cells. Nat. Immunol. *21*, 274–286.

56. Murrell, D.F., Daniel, B.S., Joly, P., Borradori, L., Amagai, M., Hashimoto, T., Caux, F., Marinovic, B., Sinha, A.A., Hertl, M., et al. (2012). Definitions and outcome measures for bullous pemphigoid: recommendations by an international panel of experts. J. Am. Acad. Dermatol. *66*, 479–485.

57. Manchanda, M., Torres, M., Inuossa, F., Bansal, R., Kumar, R., Hunt, M., Wheelock, C.E., Bachar-Wikstrom, E., and Wikstrom, J.D. (2023). Metabolic Reprogramming and Reliance in Human Skin Wound Healing. J. Invest. Dermatol. *143*, 2039–2051.e10.

58. Londe, A.C., Fernandez-Ruiz, R., Julio, P.R., Appenzeller, S., and Niewold, T.B. (2023). Type I Interferons in Autoimmunity: Implications in Clinical Phenotypes and Treatment Response. J. Rheumatol. *50*, 1103–1113.

59. Benveniste, E.N., and Qin, H. (2007). Type I interferons as anti-inflammatory mediators. Sci. STKE *2007*, e70.

60. Feng, X., Bao, R., Li, L., Deisenhammer, F., Arnason, B.G.W., and Reder, A.T. (2019). Interferon-β corrects massive gene dysregulation in multiple sclerosis: Short-term and long-term effects on immune regulation and neuroprotection. EBioMedicine *49*, 269–283.

61. Hänzelmann, S., Castelo, R., and Guinney, J. (2013). GSVA: gene set variation analysis for microarray and RNA-seq data. BMC Bioinformatics *14*, 7.

62. Stuart, T., Butler, A., Hoffman, P., Hafemeister, C., Papalexi, E., Mauck, W.M., 3rd, Hao, Y., Stoeckius, M., Smibert, P., and Satija, R. (2019). Comprehensive Integration of Single-Cell Data. Cell *177*, 1888–1902.e21.

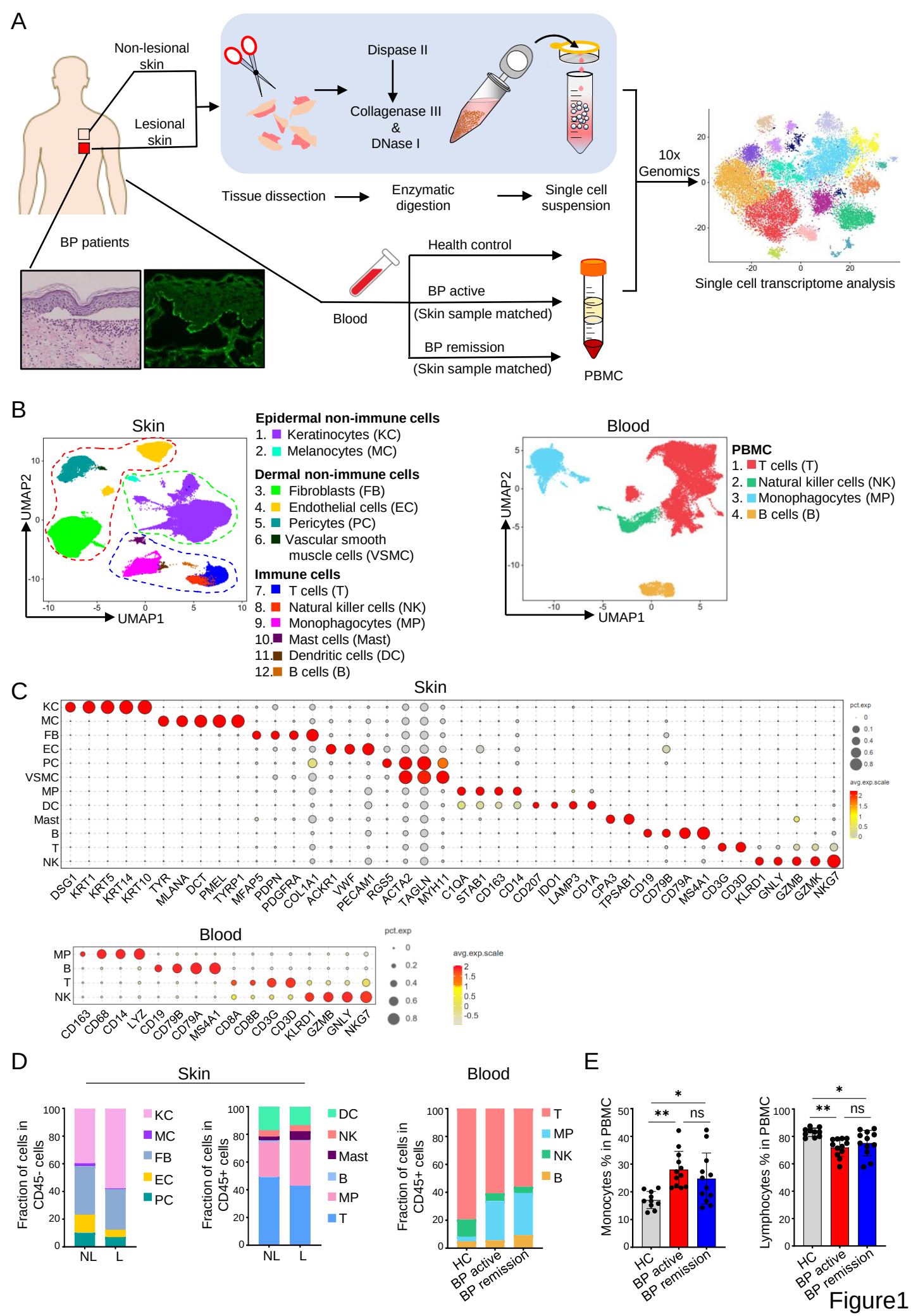
A
Non-lesional skin
Lesional skin
Dispase II
Collagenase III & DNase I
Tissue dissection
Enzymatic digestion
Single cell suspension
10x Genomics
Single cell transcriptome analysis
BP patients
Blood
Health control
BP active (Skin sample matched)
BP remission (Skin sample matched)
PBMC
B
Skin
UMAP2
UMAP1
Epidermal non-immune cells
1. Keratinocytes (KC)
2. Melanocytes (MC)
Dermal non-immune cells
3. Fibroblasts (FB)
4. Endothelial cells (EC)
5. Pericytes (PC)
6. Vascular smooth muscle cells (VSMC)
Immune cells
7. T cells (T)
8. Natural killer cells (NK)
9. Monophagocytes (MP)
10. Mast cells (Mast)
11. Dendritic cells (DC)
12. B cells (B)
Blood
PBMC
1. T cells (T)
2. Natural killer cells (NK)
3. Monophagocytes (MP)
4. B cells (B)
C
Skin
KC
MC
FB
EC
PC
VSMC
MP
DC
Mast
B
T
NK
DSG1 KRT1 KRT5 KRT14 KRT10 TYR MLANA DCT PMEL TYRP1 MFAP5 PDPN PDGFRA COL1A1 ACKR1 VWF PECAM1 RGS5 ACTA2 TAGLN MYH11 C1QA STAB1 CD163 CD14 CD207 IDO1 LAMP3 CD1A CPA3 TPSAB1 CD19 CD79B CD79A MS4A1 CD3G CD3D KLRD1 GNLY GZMB GZMK NKG7
pct.exp
avg.exp.scale
Blood
MP
B
T
NK
CD163 CD68 CD14 LYZ CD19 CD79B CD79A MS4A1 CD8A CD8B CD3G CD3D KLRD1 GZMB GNLY NKG7
D
Skin
Fraction of cells in CD45- cells
KC
MC
FB
EC
PC
NL
L
Fraction of cells in CD45+ cells
DC
NK
Mast
B
MP
T
Blood
Fraction of cells in CD45+ cells
T
MP
NK
B
HC
BP active
BP remission
E
Monocytes % in PBMC
Lymphocytes % in PBMC
**
ns
*
Figure1

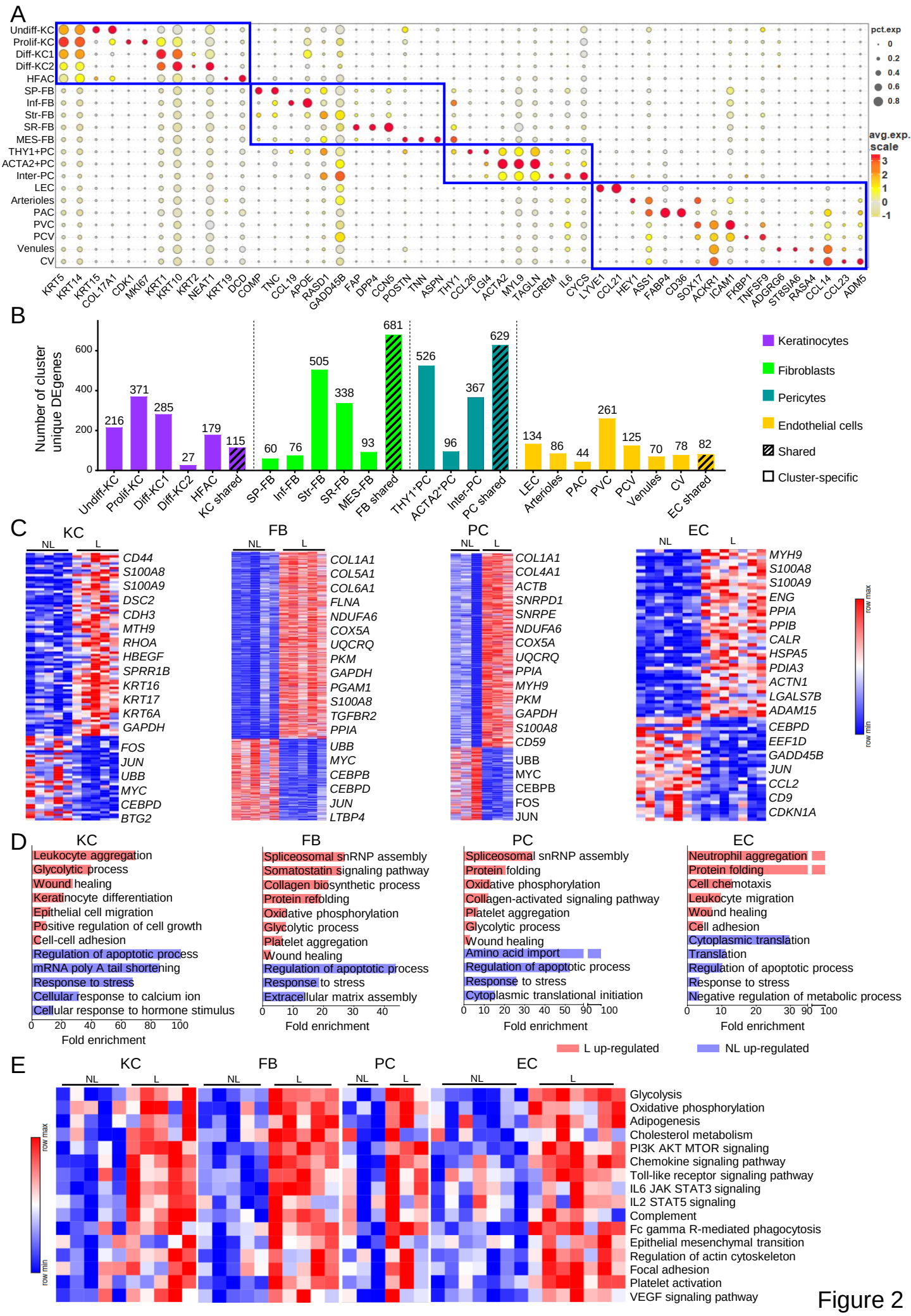
A
Undiff-KC
Prolif-KC
Diff-KC1
Diff-KC2
HFAC
SP-FB
Inf-FB
Str-FB
SR-FB
MES-FB
THY1+PC
ACTA2+PC
Inter-PC
LEC
Arterioles
PAC
PVC
PCV
Venules
CV
KRT5 KRT14 KRT15 COL17A1 CDK1 MKI67 KRT1 KRT10 KRT2 NEAT1 KRT19 DCD COMP TNC CCL19 APOE RASD1 GADD45B FAP DPP4 CCN5 POSTN TNN ASPN THY1 CCL26 LGI4 ACTA2 MYL9 TAGLN CREM IL6 CYCS LYVE1 CCL21 HEY1 ASS1 FABP4 CD36 SOX17 ACKR1 ICAM1 FKBP1 TNFSF9 ADGRG6 ST8SIA6 RASA4 CCL14 CCL23 ADM5
pct.exp
0
0.2
0.4
0.6
0.8
avg.exp. scale
3
2
1
0
-1
B
Number of cluster unique DEgenes
0
200
400
600
216
371
285
27
179
115
60
76
505
338
93
681
526
96
367
629
134
86
44
261
125
70
78
82
Undiff-KC
Prolif-KC
Diff-KC1
Diff-KC2
HFAC
KC shared
SP-FB
Inf-FB
Str-FB
SR-FB
MES-FB
FB shared
THY1+PC
ACTA2+PC
Inter-PC
PC shared
LEC
Arterioles
PAC
PVC
PCV
Venules
CV
EC shared
Keratinocytes
Fibroblasts
Pericytes
Endothelial cells
Shared
Cluster-specific
C
KC
NL
L
CD44
S100A8
S100A9
DSC2
CDH3
MTH9
RHOA
HBEGF
SPRR1B
KRT16
KRT17
KRT6A
GAPDH
FOS
JUN
UBB
MYC
CEBPD
BTG2
FB
COL1A1
COL5A1
COL6A1
FLNA
NDUFA6
COX5A
UQCRQ
PKM
GAPDH
PGAM1
S100A8
TGFBR2
PPIA
UBB
MYC
CEBPB
CEBPD
JUN
LTBP4
PC
COL1A1
COL4A1
ACTB
SNRPD1
SNRPE
NDUFA6
COX5A
UQCRQ
PPIA
MYH9
PKM
GAPDH
S100A8
CD59
UBB
MYC
CEBPB
FOS
JUN
EC
MYH9
S100A8
S100A9
ENG
PPIA
PPIB
CALR
HSPA5
PDIA3
ACTN1
LGALS7B
ADAM15
CEBPD
EEF1D
GADD45B
JUN
CCL2
CD9
CDKN1A
row max
row min
D
KC
Leukocyte aggregation
Glycolytic process
Wound healing
Keratinocyte differentiation
Epithelial cell migration
Positive regulation of cell growth
Cell-cell adhesion
Regulation of apoptotic process
mRNA poly A tail shortening
Response to stress
Cellular response to calcium ion
Cellular response to hormone stimulus
0 20 40 60 80 100
Fold enrichment
FB
Spliceosomal snRNP assembly
Somatostatin signaling pathway
Collagen biosynthetic process
Protein refolding
Oxidative phosphorylation
Glycolytic process
Platelet aggregation
Wound healing
Regulation of apoptotic process
Response to stress
Extracellular matrix assembly
0 10 20 30 40
Fold enrichment
PC
Spliceosomal snRNP assembly
Protein folding
Oxidative phosphorylation
Collagen-activated signaling pathway
Platelet aggregation
Glycolytic process
Wound healing
Amino acid import
Regulation of apoptotic process
Response to stress
Cytoplasmic translational initiation
0 10 20 30 40 50 90 100
Fold enrichment
EC
Neutrophil aggregation
Protein folding
Cell chemotaxis
Leukocyte migration
Wound healing
Cell adhesion
Cytoplasmic translation
Translation
Regulation of apoptotic process
Response to stress
Negative regulation of metabolic process
0 10 20 30 90 100
Fold enrichment
L up-regulated
NL up-regulated
E
KC
FB
PC
EC
NL
L
Glycolysis
Oxidative phosphorylation
Adipogenesis
Cholesterol metabolism
PI3K AKT MTOR signaling
Chemokine signaling pathway
Toll-like receptor signaling pathway
IL6 JAK STAT3 signaling
IL2 STAT5 signaling
Complement
Fc gamma R-mediated phagocytosis
Epithelial mesenchymal transition
Regulation of actin cytoskeleton
Focal adhesion
Platelet activation
VEGF signaling pathway
row max
row min

Figure 2

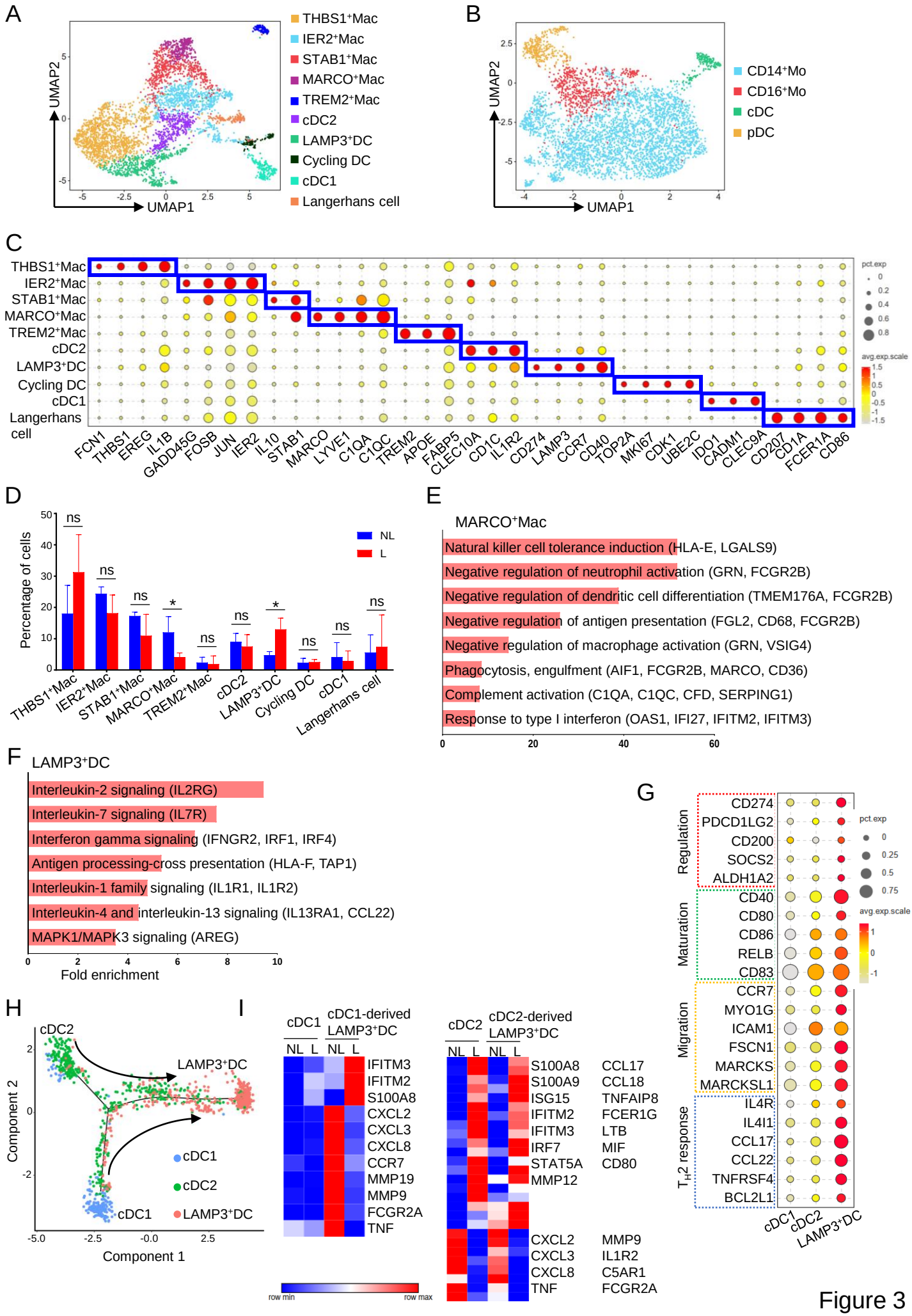
A
UMAP2
UMAP1
THBS1+Mac
IER2+Mac
STAB1+Mac
MARCO+Mac
TREM2+Mac
cDC2
LAMP3+DC
Cycling DC
cDC1
Langerhans cell
B
UMAP2
UMAP1
CD14+Mo
CD16+Mo
cDC
pDC
C
THBS1+Mac
IER2+Mac
STAB1+Mac
MARCO+Mac
TREM2+Mac
cDC2
LAMP3+DC
Cycling DC
cDC1
Langerhans cell
FCN1 THBS1 EREG IL1B GADD45G FOSB JUN IER2 IL10 STAB1 MARCO LYVE1 C1QA C1QC TREM2 APOE FABP5 CLEC10A CD1C IL1R2 CD274 LAMP3 CCR7 CD40 TOP2A MKI67 CDK1 UBE2C IDO1 CADM1 CLEC9A CD207 CD1A FCER1A CD86
pct.exp
avg.exp.scale
D
Percentage of cells
NL
L
ns
*
THBS1+Mac
IER2+Mac
STAB1+Mac
MARCO+Mac
TREM2+Mac
cDC2
LAMP3+DC
Cycling DC
cDC1
Langerhans cell
E
MARCO+Mac
Natural killer cell tolerance induction (HLA-E, LGALS9)
Negative regulation of neutrophil activation (GRN, FCGR2B)
Negative regulation of dendritic cell differentiation (TMEM176A, FCGR2B)
Negative regulation of antigen presentation (FGL2, CD68, FCGR2B)
Negative regulation of macrophage activation (GRN, VSIG4)
Phagocytosis, engulfment (AIF1, FCGR2B, MARCO, CD36)
Complement activation (C1QA, C1QC, CFD, SERPING1)
Response to type I interferon (OAS1, IFI27, IFITM2, IFITM3)
F
LAMP3+DC
Interleukin-2 signaling (IL2RG)
Interleukin-7 signaling (IL7R)
Interferon gamma signaling (IFNGR2, IRF1, IRF4)
Antigen processing-cross presentation (HLA-F, TAP1)
Interleukin-1 family signaling (IL1R1, IL1R2)
Interleukin-4 and interleukin-13 signaling (IL13RA1, CCL22)
MAPK1/MAPK3 signaling (AREG)
Fold enrichment
G
Regulation
CD274
PDCD1LG2
CD200
SOCS2
ALDH1A2
Maturation
CD40
CD80
CD86
RELB
CD83
Migration
CCR7
MYO1G
ICAM1
FSCN1
MARCKS
MARCKSL1
TH2 response
IL4R
IL4I1
CCL17
CCL22
TNFRSF4
BCL2L1
cDC1
cDC2
LAMP3+DC
pct.exp
avg.exp.scale
H
cDC2
LAMP3+DC
cDC1
cDC1
cDC2
LAMP3+DC
Component 2
Component 1
I
cDC1
cDC1-derived LAMP3+DC
NL L NL L
IFITM3
IFITM2
S100A8
CXCL2
CXCL3
CXCL8
CCR7
MMP19
MMP9
FCGR2A
TNF
cDC2
cDC2-derived LAMP3+DC
NL L NL L
S100A8
S100A9
ISG15
IFITM2
IFITM3
IRF7
STAT5A
MMP12
CXCL2
CXCL3
CXCL8
TNF
CCL17
CCL18
TNFAIP8
FCER1G
LTB
MIF
CD80
MMP9
IL1R2
C5AR1
FCGR2A
row min
row max

Figure 3

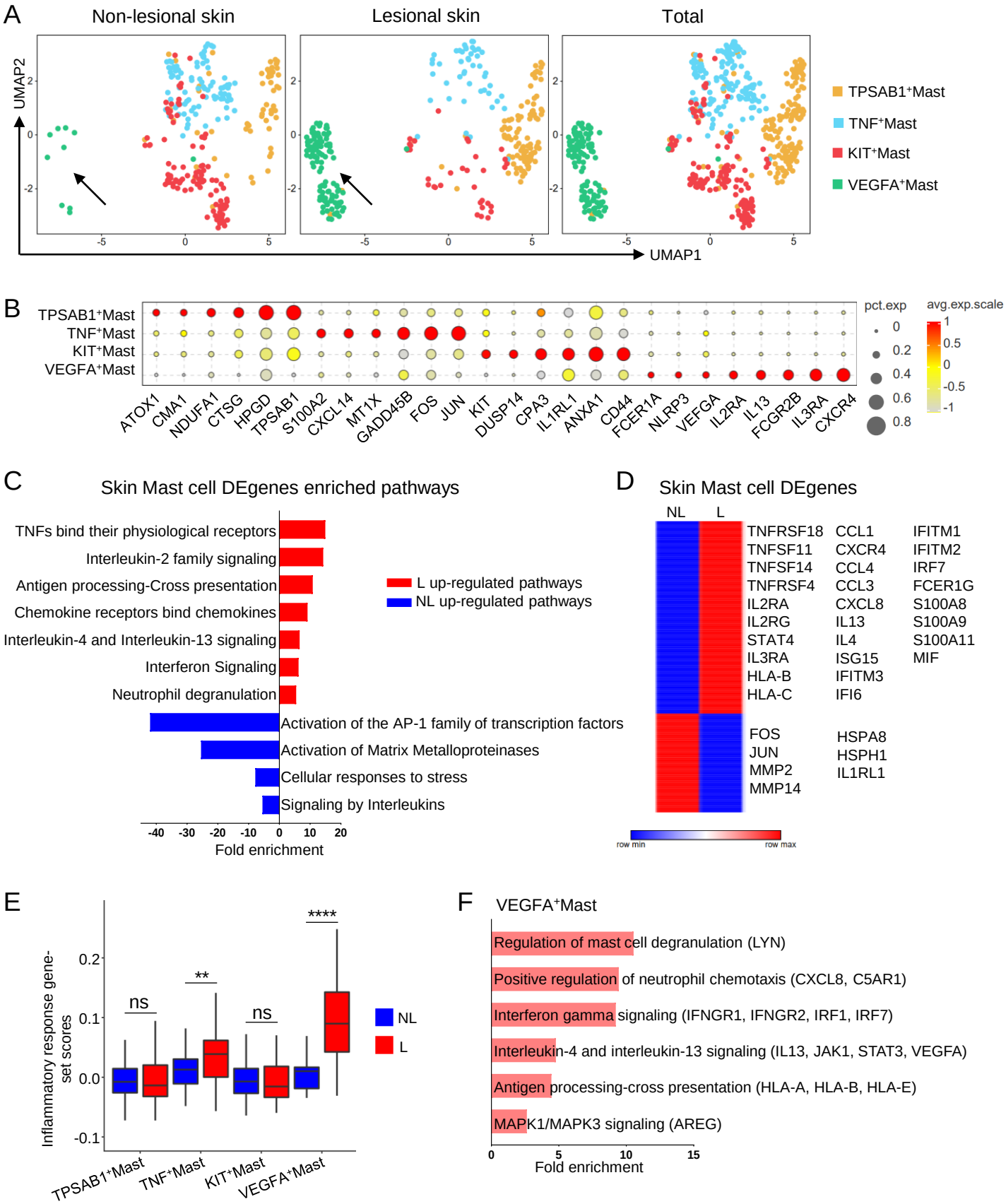
A
Non-lesional skin
Lesional skin
Total
UMAP2
UMAP1
TPSAB1+Mast
TNF+Mast
KIT+Mast
VEGFA+Mast
B
TPSAB1+Mast
TNF+Mast
KIT+Mast
VEGFA+Mast
ATOX1
CMA1
NDUFA1
CTSG
HPGD
TPSAB1
S100A2
CXCL14
MT1X
GADD45B
FOS
JUN
KIT
DUSP14
CPA3
IL1RL1
ANXA1
CD44
FCER1A
NLRP3
VEFGA
IL2RA
IL13
FCGR2B
IL3RA
CXCR4
pct.exp
avg.exp.scale
C
Skin Mast cell DEgenes enriched pathways
TNFs bind their physiological receptors
Interleukin-2 family signaling
Antigen processing-Cross presentation
Chemokine receptors bind chemokines
Interleukin-4 and Interleukin-13 signaling
Interferon Signaling
Neutrophil degranulation
Activation of the AP-1 family of transcription factors
Activation of Matrix Metalloproteinases
Cellular responses to stress
Signaling by Interleukins
L up-regulated pathways
NL up-regulated pathways
Fold enrichment
D
Skin Mast cell DEgenes
NL
L
TNFRSF18
TNFSF11
TNFSF14
TNFRSF4
IL2RA
IL2RG
STAT4
IL3RA
HLA-B
HLA-C
CCL1
CXCR4
CCL4
CCL3
CXCL8
IL13
IL4
ISG15
IFITM3
IFI6
IFITM1
IFITM2
IRF7
FCER1G
S100A8
S100A9
S100A11
MIF
FOS
JUN
MMP2
MMP14
HSPA8
HSPH1
IL1RL1
row min
row max
E
Inflammatory response gene-set scores
ns
**
ns
****
NL
L
TPSAB1+Mast
TNF+Mast
KIT+Mast
VEGFA+Mast
F
VEGFA+Mast
Regulation of mast cell degranulation (LYN)
Positive regulation of neutrophil chemotaxis (CXCL8, C5AR1)
Interferon gamma signaling (IFNGR1, IFNGR2, IRF1, IRF7)
Interleukin-4 and interleukin-13 signaling (IL13, JAK1, STAT3, VEGFA)
Antigen processing-cross presentation (HLA-A, HLA-B, HLA-E)
MAPK1/MAPK3 signaling (AREG)
Fold enrichment

Figure 4

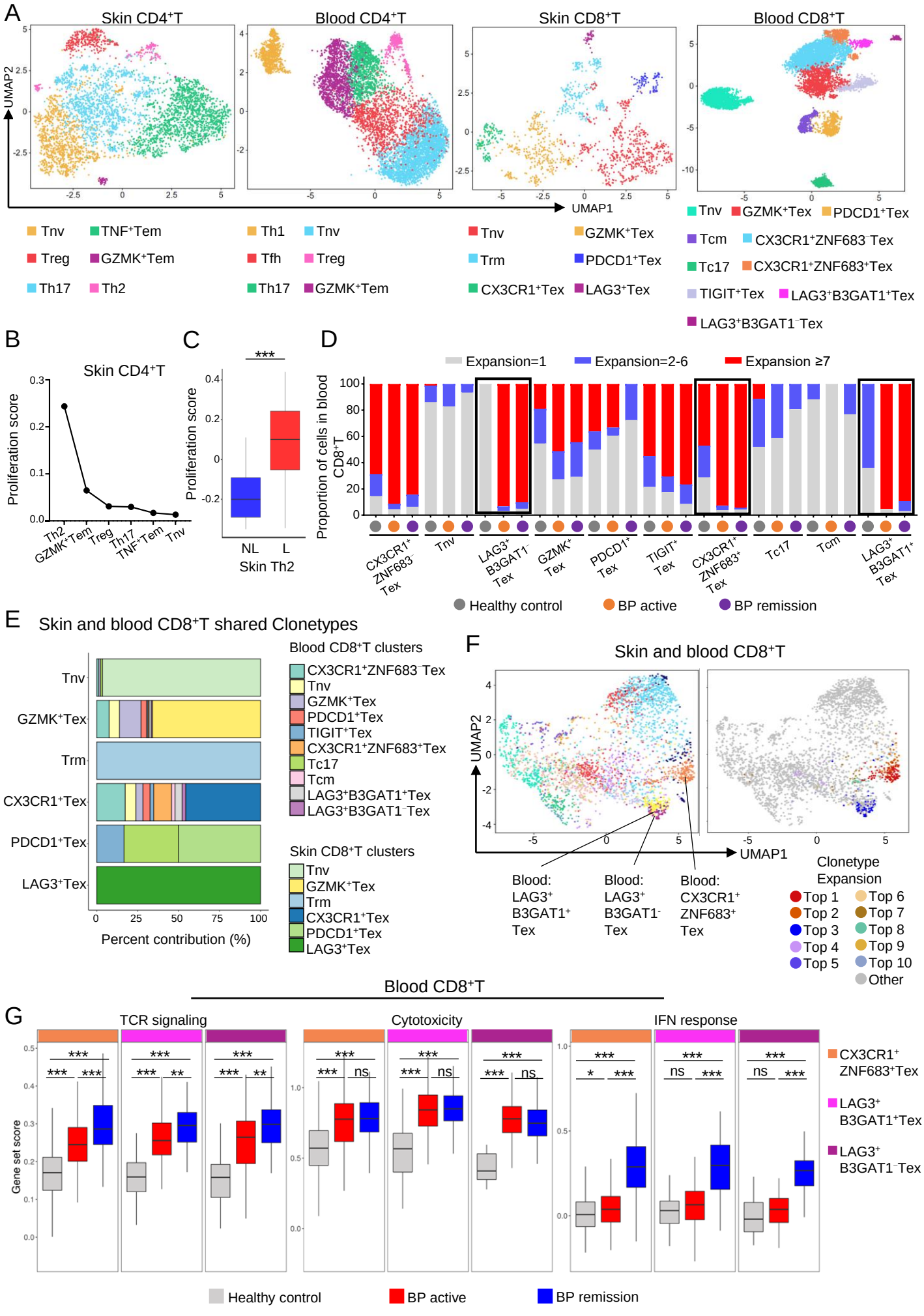
A
Skin CD4+T
Blood CD4+T
Skin CD8+T
Blood CD8+T
UMAP2
UMAP1
Tnv
TNF+Tem
Treg
GZMK+Tem
Th17
Th2
Th1
Tfh
GZMK+Tem
GZMK+Tex
Trm
PDCD1+Tex
CX3CR1+Tex
LAG3+Tex
Tcm
CX3CR1+ZNF683-Tex
Tc17
CX3CR1+ZNF683+Tex
TIGIT+Tex
LAG3+B3GAT1+Tex
LAG3+B3GAT1-Tex
B
Skin CD4+T
Proliferation score
Th2
GZMK+Tem
Treg
Th17
TNF+Tem
Tnv
C
***
Proliferation score
NL
L
Skin Th2
D
Expansion=1
Expansion=2-6
Expansion ≥7
Proportion of cells in blood CD8+T
CX3CR1+ ZNF683- Tex
Tnv
LAG3+ B3GAT1- Tex
GZMK+ Tex
PDCD1+ Tex
TIGIT+ Tex
CX3CR1+ ZNF683+ Tex
Tc17
Tcm
LAG3+ B3GAT1+ Tex
Healthy control
BP active
BP remission
E
Skin and blood CD8+T shared Clonetypes
Tnv
GZMK+Tex
Trm
CX3CR1+Tex
PDCD1+Tex
LAG3+Tex
Percent contribution (%)
Blood CD8+T clusters
CX3CR1+ZNF683-Tex
Tnv
GZMK+Tex
PDCD1+Tex
TIGIT+Tex
CX3CR1+ZNF683+Tex
Tc17
Tcm
LAG3+B3GAT1+Tex
LAG3+B3GAT1-Tex
Skin CD8+T clusters
Tnv
GZMK+Tex
Trm
CX3CR1+Tex
PDCD1+Tex
LAG3+Tex
F
Skin and blood CD8+T
UMAP2
UMAP1
Blood: LAG3+ B3GAT1+ Tex
Blood: LAG3+ B3GAT1- Tex
Blood: CX3CR1+ ZNF683+ Tex
Clonetype Expansion
Top 1
Top 2
Top 3
Top 4
Top 5
Top 6
Top 7
Top 8
Top 9
Top 10
Other
Blood CD8+T
G
TCR signaling
Cytotoxicity
IFN response
Gene set score
CX3CR1+ ZNF683+Tex
LAG3+ B3GAT1+Tex
LAG3+ B3GAT1-Tex
Healthy control
BP active
BP remission

Figure 5

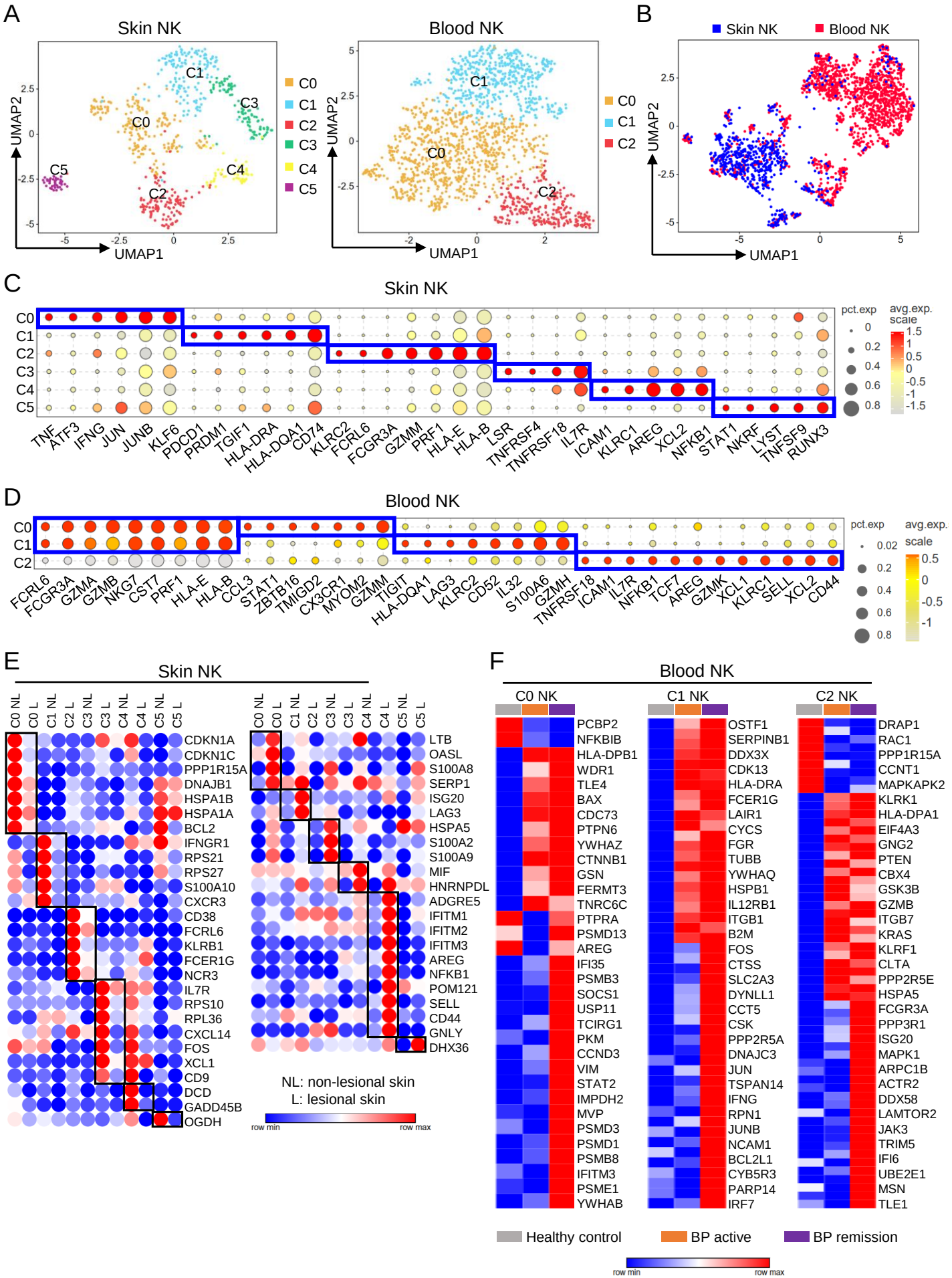
A
Skin NK
Blood NK
UMAP1
UMAP2
C0
C1
C2
C3
C4
C5
B
Skin NK
Blood NK
C
Skin NK
pct.exp
avg.exp.
scale
TNF ATF3 IFNG JUN JUNB KLF6 PDCD1 PRDM1 TGIF1 HLA-DRA HLA-DQA1 CD74 KLRC2 FCRL6 FCGR3A GZMM PRF1 HLA-E HLA-B LSR TNFRSF4 TNFRSF18 IL7R ICAM1 KLRC1 AREG XCL2 NFKB1 STAT1 NKRF LYST TNFSF9 RUNX3
D
Blood NK
FCRL6 FCGR3A GZMA GZMB NKG7 CST7 PRF1 HLA-E HLA-B CCL3 STAT1 ZBTB16 TMIGD2 CX3CR1 MYOM2 GZMM TIGIT HLA-DQA1 LAG3 KLRC2 CD52 IL32 S100A6 GZMH TNFRSF18 ICAM1 IL7R NFKB1 TCF7 AREG GZMK XCL1 KLRC1 SELL XCL2 CD44
E
Skin NK
C0 NL C0 L C1 NL C2 L C3 NL C3 L C4 NL C4 L C5 NL C5 L
CDKN1A CDKN1C PPP1R15A DNAJB1 HSPA1B HSPA1A BCL2 IFNGR1 RPS21 RPS27 S100A10 CXCR3 CD38 FCRL6 KLRB1 FCER1G NCR3 IL7R RPS10 RPL36 CXCL14 FOS XCL1 CD9 DCD GADD45B OGDH
LTB OASL S100A8 SERP1 ISG20 LAG3 HSPA5 S100A2 S100A9 MIF HNRNPDL ADGRE5 IFITM1 IFITM2 IFITM3 AREG NFKB1 POM121 SELL CD44 GNLY DHX36
NL: non-lesional skin
L: lesional skin
row min
row max
F
Blood NK
C0 NK
PCBP2 NFKBIB HLA-DPB1 WDR1 TLE4 BAX CDC73 PTPN6 YWHAZ CTNNB1 GSN FERMT3 TNRC6C PTPRA PSMD13 AREG IFI35 PSMB3 SOCS1 USP11 TCIRG1 PKM CCND3 VIM STAT2 IMPDH2 MVP PSMD3 PSMD1 PSMB8 IFITM3 PSME1 YWHAB
C1 NK
OSTF1 SERPINB1 DDX3X CDK13 HLA-DRA FCER1G LAIR1 CYCS FGR TUBB YWHAQ HSPB1 IL12RB1 ITGB1 B2M FOS CTSS SLC2A3 DYNLL1 CCT5 CSK PPP2R5A DNAJC3 JUN TSPAN14 IFNG RPN1 JUNB NCAM1 BCL2L1 CYB5R3 PARP14 IRF7
C2 NK
DRAP1 RAC1 PPP1R15A CCNT1 MAPKAPK2 KLRK1 HLA-DPA1 EIF4A3 GNG2 PTEN CBX4 GSK3B GZMB ITGB7 KRAS KLRF1 CLTA PPP2R5E HSPA5 FCGR3A PPP3R1 ISG20 MAPK1 ARPC1B ACTR2 DDX58 LAMTOR2 JAK3 TRIM5 IFI6 UBE2E1 MSN TLE1
Healthy control
BP active
BP remission
row min
row max

Figure 6

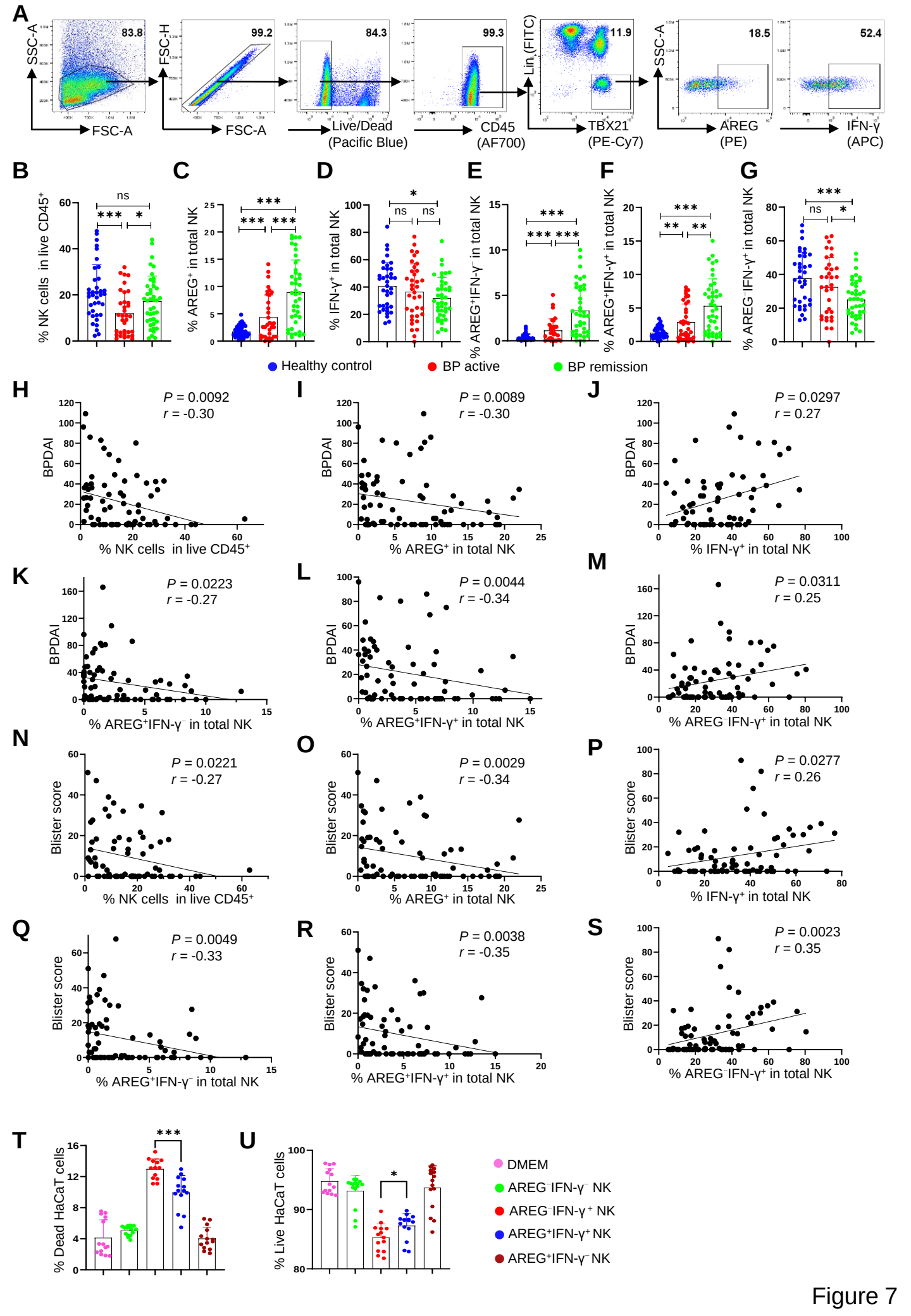
A
SSC-A
FSC-A
83.8
FSC-H
FSC-A
99.2
Live/Dead (Pacific Blue)
84.3
CD45 (AF700)
99.3
Lin (FITC)
TBX21 (PE-Cy7)
11.9
SSC-A
AREG (PE)
18.5
IFN-γ (APC)
52.4
B
% NK cells in live CD45+
C
% AREG+ in total NK
D
% IFN-γ+ in total NK
E
% AREG+IFN-γ- in total NK
F
% AREG+IFN-γ+ in total NK
G
% AREG-IFN-γ+ in total NK
Healthy control
BP active
BP remission
H
P = 0.0092
r = -0.30
BPDAI
% NK cells in live CD45+
I
P = 0.0089
r = -0.30
BPDAI
% AREG+ in total NK
J
P = 0.0297
r = 0.27
BPDAI
% IFN-γ+ in total NK
K
P = 0.0223
r = -0.27
BPDAI
% AREG+IFN-γ- in total NK
L
P = 0.0044
r = -0.34
BPDAI
% AREG+IFN-γ+ in total NK
M
P = 0.0311
r = 0.25
BPDAI
% AREG-IFN-γ+ in total NK
N
P = 0.0221
r = -0.27
Blister score
% NK cells in live CD45+
O
P = 0.0029
r = -0.34
Blister score
% AREG+ in total NK
P
P = 0.0277
r = 0.26
Blister score
% IFN-γ+ in total NK
Q
P = 0.0049
r = -0.33
Blister score
% AREG+IFN-γ- in total NK
R
P = 0.0038
r = -0.35
Blister score
% AREG+IFN-γ+ in total NK
S
P = 0.0023
r = 0.35
Blister score
% AREG-IFN-γ+ in total NK
T
% Dead HaCaT cells
U
% Live HaCaT cells
DMEM
AREG-IFN-γ- NK
AREG-IFN-γ+ NK
AREG+IFN-γ+ NK
AREG+IFN-γ- NK

Figure 7

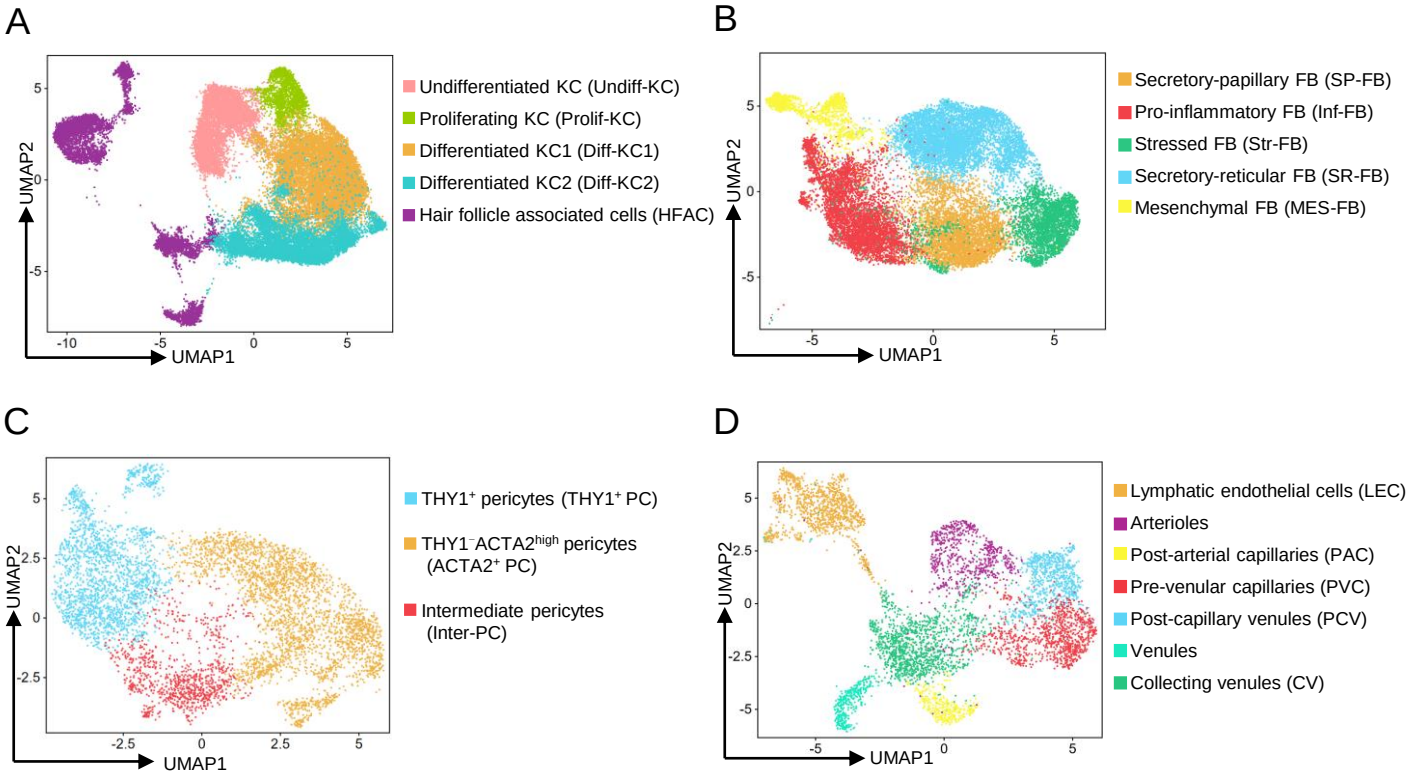
A
UMAP2
UMAP1
Undifferentiated KC (Undiff-KC)
Proliferating KC (Prolif-KC)
Differentiated KC1 (Diff-KC1)
Differentiated KC2 (Diff-KC2)
Hair follicle associated cells (HFAC)
B
UMAP2
UMAP1
Secretory-papillary FB (SP-FB)
Pro-inflammatory FB (Inf-FB)
Stressed FB (Str-FB)
Secretory-reticular FB (SR-FB)
Mesenchymal FB (MES-FB)
C
UMAP2
UMAP1
THY1+ pericytes (THY1+ PC)
THY1-ACTA2high pericytes (ACTA2+ PC)
Intermediate pericytes (Inter-PC)
D
UMAP2
UMAP1
Lymphatic endothelial cells (LEC)
Arterioles
Post-arterial capillaries (PAC)
Pre-venular capillaries (PVC)
Post-capillary venules (PCV)
Venules
Collecting venules (CV)

Figure S1

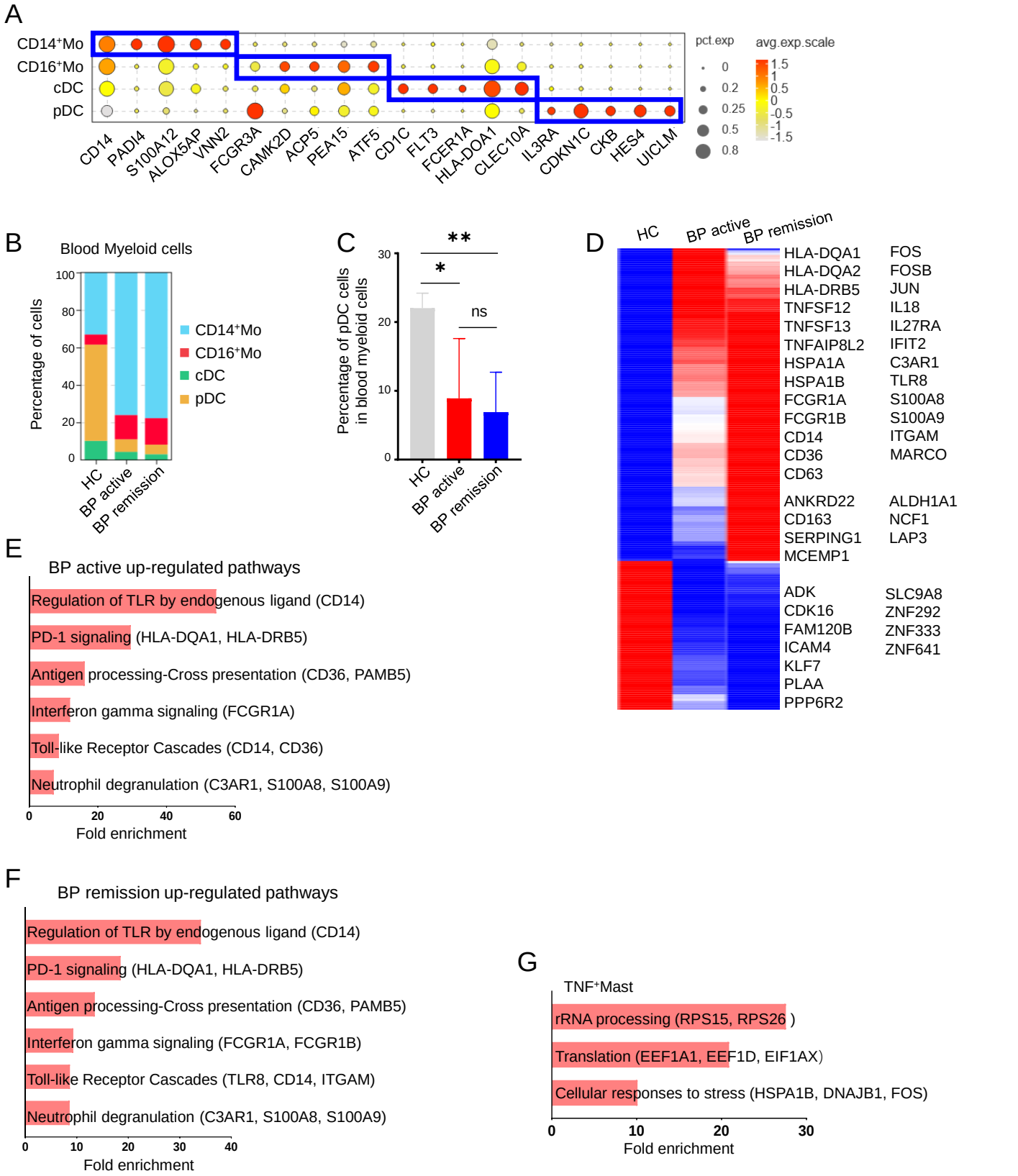
A
CD14⁺Mo
CD16⁺Mo
cDC
pDC
CD14
PADI4
S100A12
ALOX5AP
VNN2
FCGR3A
CAMK2D
ACP5
PEA15
ATF5
CD1C
FLT3
FCER1A
HLA-DOA1
CLEC10A
IL3RA
CDKN1C
CKB
HES4
UICLM
pct.exp
0
0.2
0.25
0.5
0.8
avg.exp.scale
1.5
1
0.5
0
-0.5
-1
-1.5
B
Blood Myeloid cells
Percentage of cells
100
80
60
40
20
0
CD14⁺Mo
CD16⁺Mo
cDC
pDC
HC
BP active
BP remission
C
Percentage of pDC cells in blood myeloid cells
30
20
10
0
**
*
ns
HC
BP active
BP remission
D
HC
BP active
BP remission
HLA-DQA1
HLA-DQA2
HLA-DRB5
TNFSF12
TNFSF13
TNFAIP8L2
HSPA1A
HSPA1B
FCGR1A
FCGR1B
CD14
CD36
CD63
ANKRD22
CD163
SERPING1
MCEMP1
ADK
CDK16
FAM120B
ICAM4
KLF7
PLAA
PPP6R2
FOS
FOSB
JUN
IL18
IL27RA
IFIT2
C3AR1
TLR8
S100A8
S100A9
ITGAM
MARCO
ALDH1A1
NCF1
LAP3
SLC9A8
ZNF292
ZNF333
ZNF641
E
BP active up-regulated pathways
Regulation of TLR by endogenous ligand (CD14)
PD-1 signaling (HLA-DQA1, HLA-DRB5)
Antigen processing-Cross presentation (CD36, PAMB5)
Interferon gamma signaling (FCGR1A)
Toll-like Receptor Cascades (CD14, CD36)
Neutrophil degranulation (C3AR1, S100A8, S100A9)
0
20
40
60
Fold enrichment
F
BP remission up-regulated pathways
Regulation of TLR by endogenous ligand (CD14)
PD-1 signaling (HLA-DQA1, HLA-DRB5)
Antigen processing-Cross presentation (CD36, PAMB5)
Interferon gamma signaling (FCGR1A, FCGR1B)
Toll-like Receptor Cascades (TLR8, CD14, ITGAM)
Neutrophil degranulation (C3AR1, S100A8, S100A9)
0
10
20
30
40
Fold enrichment
G
TNF⁺Mast
rRNA processing (RPS15, RPS26)
Translation (EEF1A1, EEF1D, EIF1AX)
Cellular responses to stress (HSPA1B, DNAJB1, FOS)
0
10
20
30
Fold enrichment

Figure S2

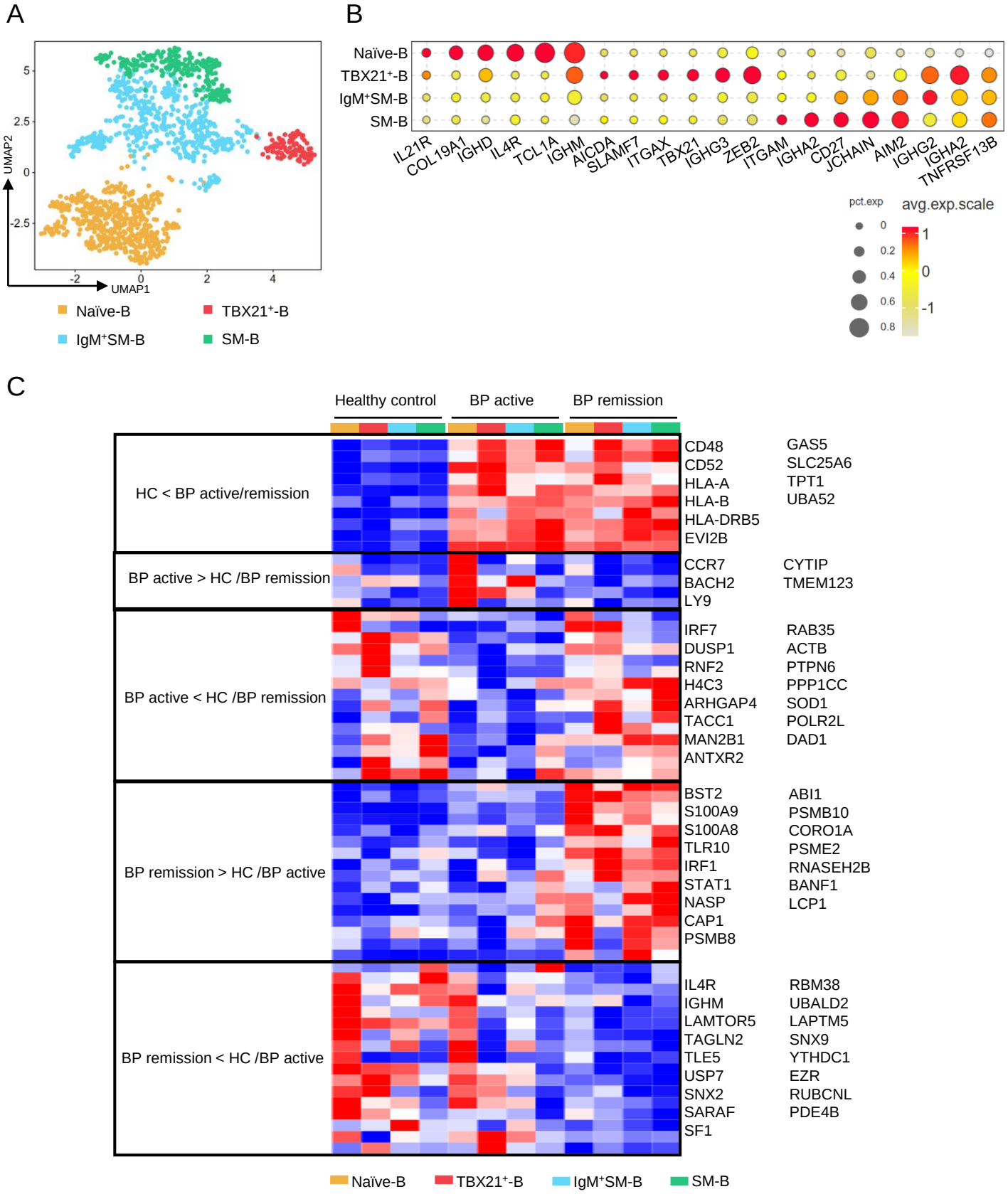
A
UMAP2
UMAP1
Naïve-B
TBX21+-B
IgM+SM-B
SM-B
B
Naïve-B
TBX21+-B
IgM+SM-B
SM-B
IL21R
COL19A1
IGHD
IL4R
TCL1A
IGHM
AICDA
SLAMF7
ITGAX
TBX21
IGHG3
ZEB2
ITGAM
IGHA2
CD27
JCHAIN
AIM2
IGHG2
IGHA2
TNFRSF13B
pct.exp
avg.exp.scale
C
Healthy control
BP active
BP remission
HC < BP active/remission
CD48
CD52
HLA-A
HLA-B
HLA-DRB5
EVI2B
GAS5
SLC25A6
TPT1
UBA52
BP active > HC /BP remission
CCR7
BACH2
LY9
CYTIP
TMEM123
BP active < HC /BP remission
IRF7
DUSP1
RNF2
H4C3
ARHGAP4
TACC1
MAN2B1
ANTXR2
RAB35
ACTB
PTPN6
PPP1CC
SOD1
POLR2L
DAD1
BP remission > HC /BP active
BST2
S100A9
S100A8
TLR10
IRF1
STAT1
NASP
CAP1
PSMB8
ABI1
PSMB10
CORO1A
PSME2
RNASEH2B
BANF1
LCP1
BP remission < HC /BP active
IL4R
IGHM
LAMTOR5
TAGLN2
TLE5
USP7
SNX2
SARAF
SF1
RBM38
UBALD2
LAPTM5
SNX9
YTHDC1
EZR
RUBCNL
PDE4B
Naïve-B
TBX21+-B
IgM+SM-B
SM-B

Figure S3

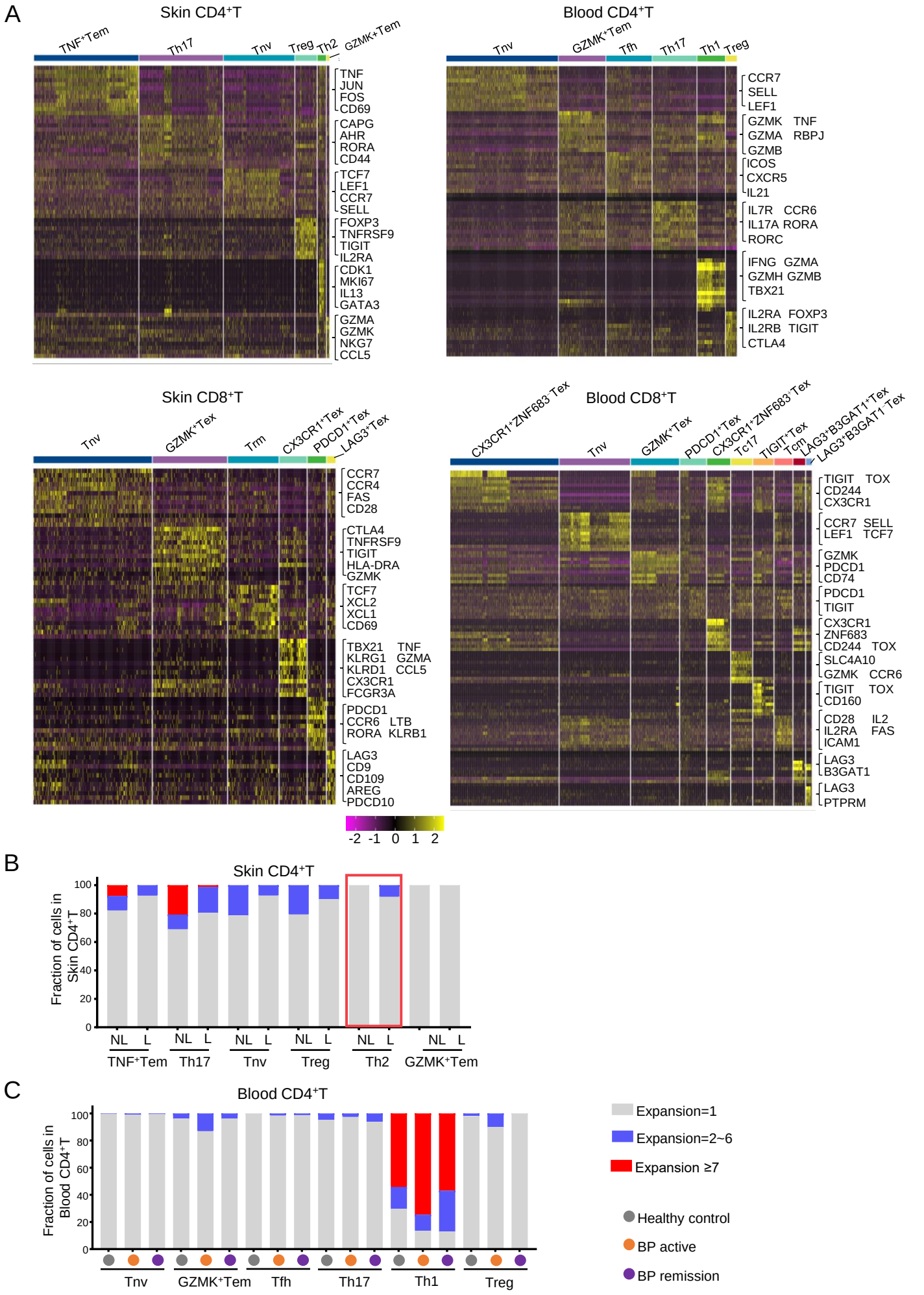
A
Skin CD4+T
TNF+Tem
Th17
Tnv
Treg
Th2
GZMK+Tem
TNF
JUN
FOS
CD69
CAPG
AHR
RORA
CD44
TCF7
LEF1
CCR7
SELL
FOXP3
TNFRSF9
TIGIT
IL2RA
CDK1
MKI67
IL13
GATA3
GZMA
GZMK
NKG7
CCL5
Blood CD4+T
Tnv
GZMK+Tem
Tfh
Th17
Th1
Treg
CCR7
SELL
LEF1
GZMK TNF
GZMA RBPJ
GZMB
ICOS
CXCR5
IL21
IL7R CCR6
IL17A RORA
RORC
IFNG GZMA
GZMH GZMB
TBX21
IL2RA FOXP3
IL2RB TIGIT
CTLA4
Skin CD8+T
Tnv
GZMK+Tex
Trm
CX3CR1+Tex
PDCD1+Tex
LAG3+Tex
CCR7
CCR4
FAS
CD28
CTLA4
TNFRSF9
TIGIT
HLA-DRA
GZMK
TCF7
XCL2
XCL1
CD69
TBX21 TNF
KLRG1 GZMA
KLRD1 CCL5
CX3CR1
FCGR3A
PDCD1
CCR6 LTB
RORA KLRB1
LAG3
CD9
CD109
AREG
PDCD10
-2 -1 0 1 2
Blood CD8+T
CX3CR1+ZNF683-Tex
Tnv
GZMK+Tex
PDCD1+Tex
CX3CR1+ZNF683+Tex
Tc17
TIGIT+Tex
Tcm
LAG3+B3GAT1+Tex
LAG3+B3GAT1-Tex
TIGIT TOX
CD244
CX3CR1
CCR7 SELL
LEF1 TCF7
GZMK
PDCD1
CD74
PDCD1
TIGIT
CX3CR1
ZNF683
CD244 TOX
SLC4A10
GZMK CCR6
TIGIT TOX
CD160
CD28 IL2
IL2RA FAS
ICAM1
LAG3
B3GAT1
LAG3
PTPRM
B
Skin CD4+T
Fraction of cells in Skin CD4+T
100
80
60
40
20
0
NL L
TNF+Tem
Th17
Tnv
Treg
Th2
GZMK+Tem
C
Blood CD4+T
Fraction of cells in Blood CD4+T
Tnv
GZMK+Tem
Tfh
Th17
Th1
Treg
Expansion=1
Expansion=2~6
Expansion ≥7
Healthy control
BP active
BP remission

Figure S4

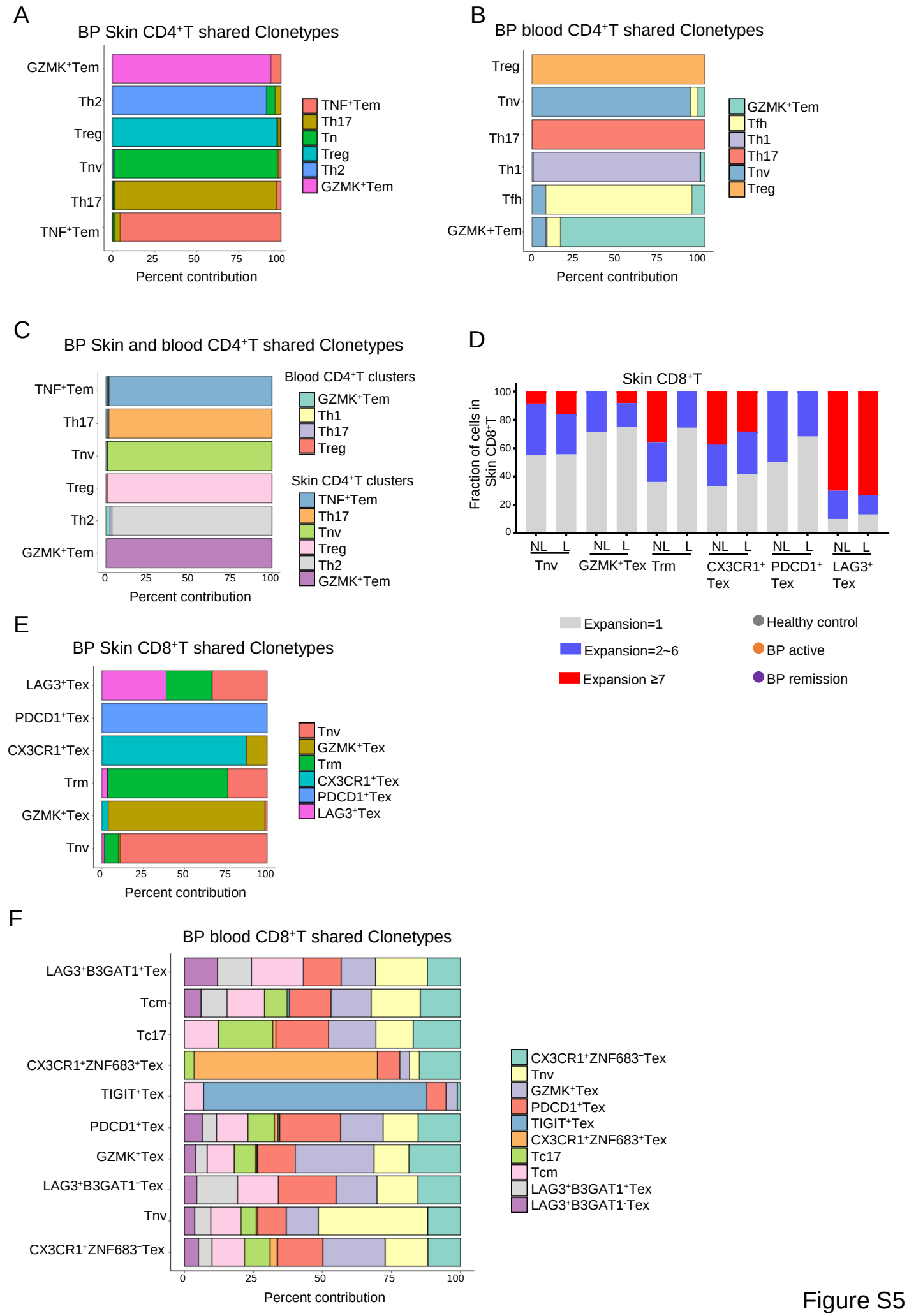
A
BP Skin CD4+T shared Clonetypes
GZMK+Tem
Th2
Treg
Tnv
Th17
TNF+Tem
0
25
50
75
100
Percent contribution
TNF+Tem
Th17
Tn
Treg
Th2
GZMK+Tem
B
BP blood CD4+T shared Clonetypes
Treg
Tnv
Th17
Th1
Tfh
GZMK+Tem
0
25
50
75
100
Percent contribution
GZMK+Tem
Tfh
Th1
Th17
Tnv
Treg
C
BP Skin and blood CD4+T shared Clonetypes
TNF+Tem
Th17
Tnv
Treg
Th2
GZMK+Tem
0
25
50
75
100
Percent contribution
Blood CD4+T clusters
GZMK+Tem
Th1
Th17
Treg
Skin CD4+T clusters
TNF+Tem
Th17
Tnv
Treg
Th2
GZMK+Tem
D
Skin CD8+T
Fraction of cells in Skin CD8+T
100
80
60
40
20
0
NL L
Tnv
NL L
GZMK+Tex
NL L
Trm
NL L
CX3CR1+ Tex
NL L
PDCD1+ Tex
NL L
LAG3+ Tex
Expansion=1
Expansion=2~6
Expansion ≥7
Healthy control
BP active
BP remission
E
BP Skin CD8+T shared Clonetypes
LAG3+Tex
PDCD1+Tex
CX3CR1+Tex
Trm
GZMK+Tex
Tnv
0
25
50
75
100
Percent contribution
Tnv
GZMK+Tex
Trm
CX3CR1+Tex
PDCD1+Tex
LAG3+Tex
F
BP blood CD8+T shared Clonetypes
LAG3+B3GAT1+Tex
Tcm
Tc17
CX3CR1+ZNF683+Tex
TIGIT+Tex
PDCD1+Tex
GZMK+Tex
LAG3+B3GAT1-Tex
Tnv
CX3CR1+ZNF683-Tex
0
25
50
75
100
Percent contribution
CX3CR1+ZNF683-Tex
Tnv
GZMK+Tex
PDCD1+Tex
TIGIT+Tex
CX3CR1+ZNF683+Tex
Tc17
Tcm
LAG3+B3GAT1+Tex
LAG3+B3GAT1-Tex

Figure S5

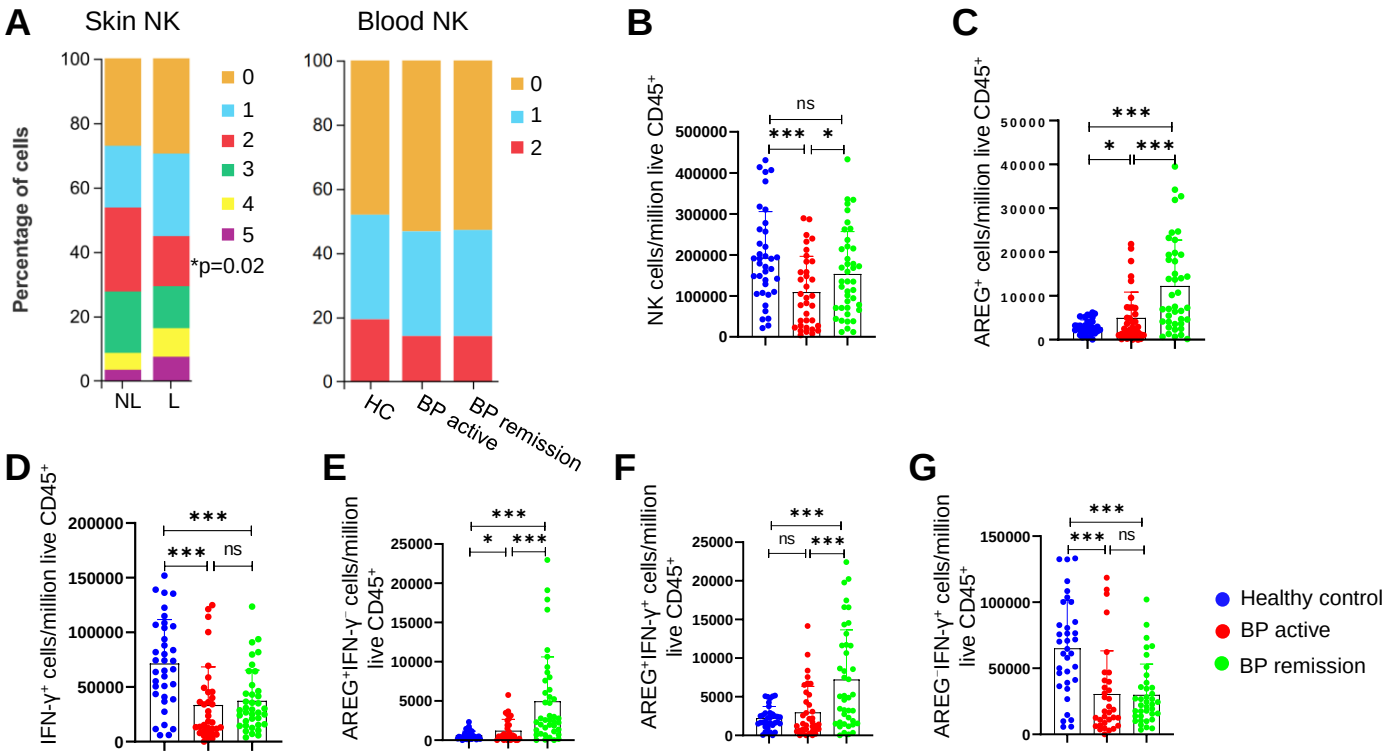
A
Skin NK
Blood NK
Percentage of cells
0
1
2
3
4
5
*p=0.02
NL
L
HC
BP active
BP remission
B
NK cells/million live CD45+
ns
***
*
C
AREG+ cells/million live CD45+
D
IFN-γ+ cells/million live CD45+
E
AREG+IFN-γ- cells/million live CD45+
F
AREG+IFN-γ+ cells/million live CD45+
G
AREG-IFN-γ+ cells/million live CD45+
Healthy control
BP active
BP remission

Figure S6

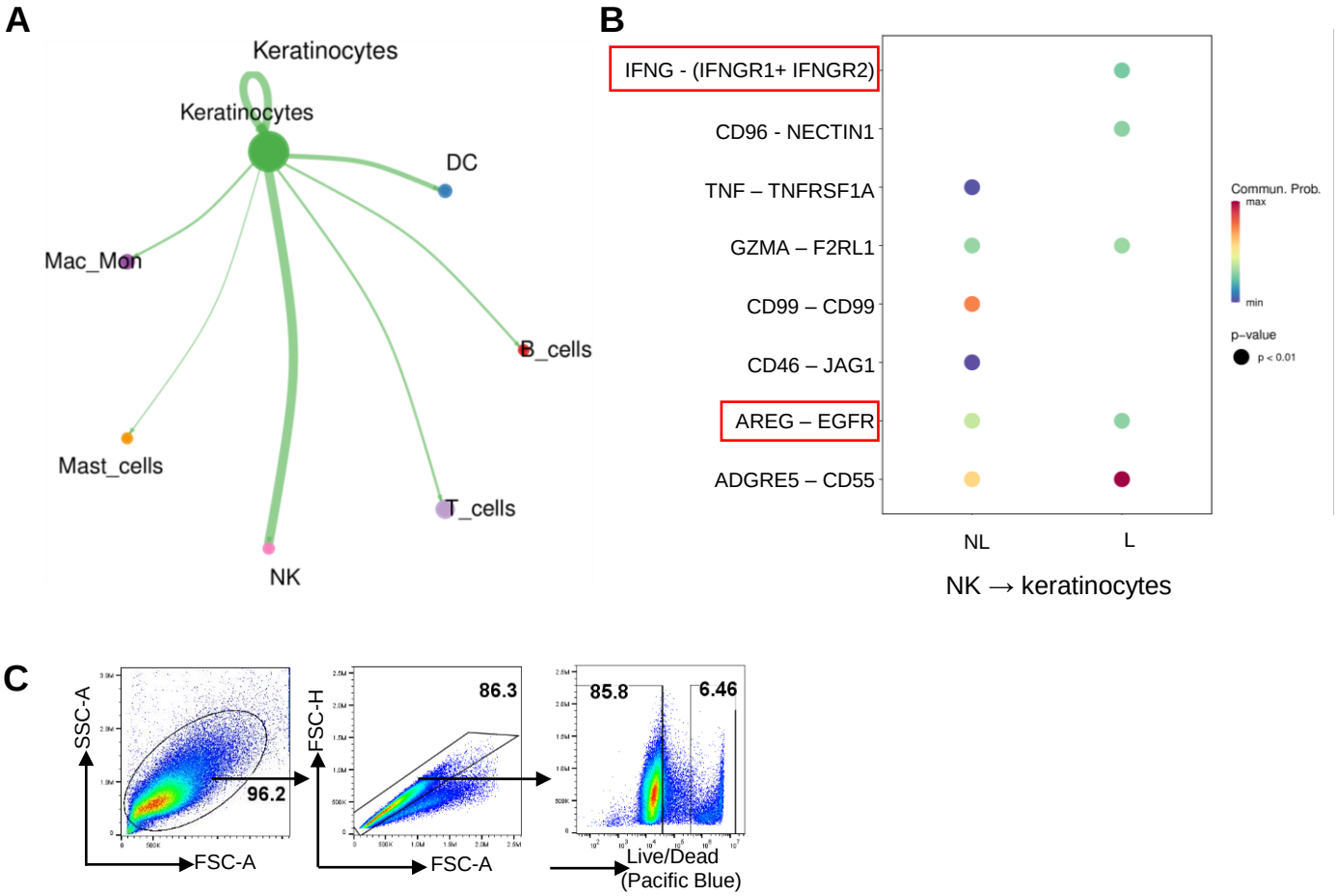
A
Keratinocytes
Keratinocytes
DC
Mac_Mon
B_cells
Mast_cells
T_cells
NK
B
IFNG - (IFNGR1+ IFNGR2)
CD96 - NECTIN1
TNF – TNFRSF1A
GZMA – F2RL1
CD99 – CD99
CD46 – JAG1
AREG – EGFR
ADGRE5 – CD55
NL
L
NK → keratinocytes
Commun. Prob.
max
min
p–value
p < 0.01
C
SSC-A
FSC-A
96.2
FSC-H
FSC-A
86.3
85.8
6.46
Live/Dead
(Pacific Blue)

Figure S7